Capella
as a
calibration target

Vinay Kashyap
Jennifer Posson-Brown
Jeremy Drake
(CfA/CXC)

alpha Auriga

transiting even as we speak

Capella
as an
EUV/X-ray target

1979-03-02	Einstein/HRI
1979-03-14	Einstein/HRI
1979-03-18	Einstein/FPCS
1979-03-19	Einstein/FPCS
1979-03-21	Einstein/FPCS
1979-03-22	Einstein/FPCS
1979-03-22	Einstein/FPCS
1979-09-12	Einstein/FPCS
1979-09-13	Einstein/FPCS
1979-09-20	Einstein/IPC

plus 106 with IUE

~150 observations with *Einstein*, ASCA, ROSAT, EUVE, *BeppoSAX*, XMM-*Newton*, and *Chandra*

plus 106 with IUE

why?

ROSAT count rate ~24 ct/s

primary G8 is a clump giant and secondary G1 is a gap giant

Emission Line Project

30 km/s and 3 km/s

why?

- brightest accessible coronal source
- interesting evolutionary status
- line dominated spectrum
- no peculiar velocity dispersions
- multi-thermal, but large $T=10^{6.8}$ K component
- stable. no flares. ever. so far.

ROSAT count rate ~24 ct/s

primary G8 is a clump giant and secondary G1 is a gap giant

Emission Line Project

30 km/s and 3 km/s

CAPELLA

α Aur / HD 34029 / HR 1708 / SAO 40186 / 13 Aur

distance = 13.4 pc

period = 104 days

inclination = 41 deg

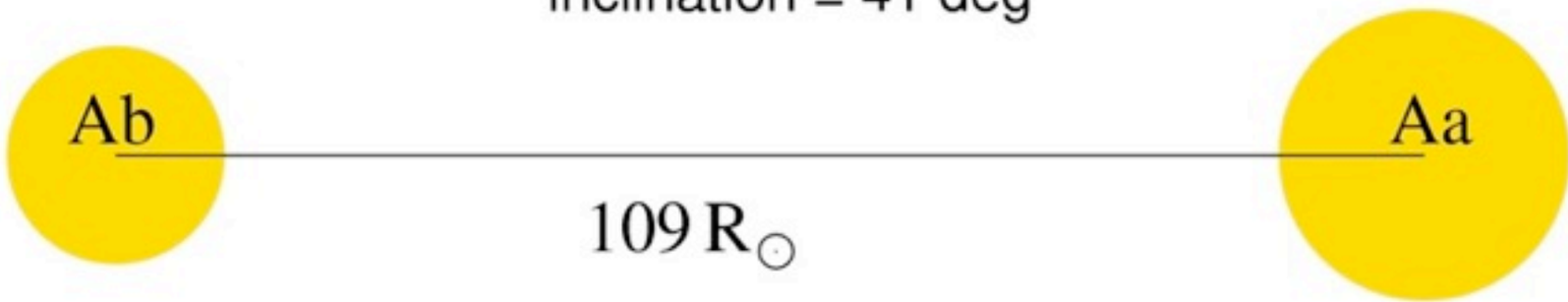

G1 III

(F9 III)

Mass = 2.56 M☉

radius = 9.2 R☉

Teff = 5700 K

B–V = 0.74

Mv = 0.14

rotation= 36 km/s

↔ 10 R☉

G8 III

(K0 III)

Mass = 2.69 M☉

radius = 12.2 R☉

Teff = 4940 K

B–V = 0.87

Mv = 0.25

rotation= 3 km/s

separation is approx 40 mas
diameters are approx 6-7 mas
Strassmeier claims Aa is tidally locked, but period from (2piR/vrot) is 205d, more like 2:1?

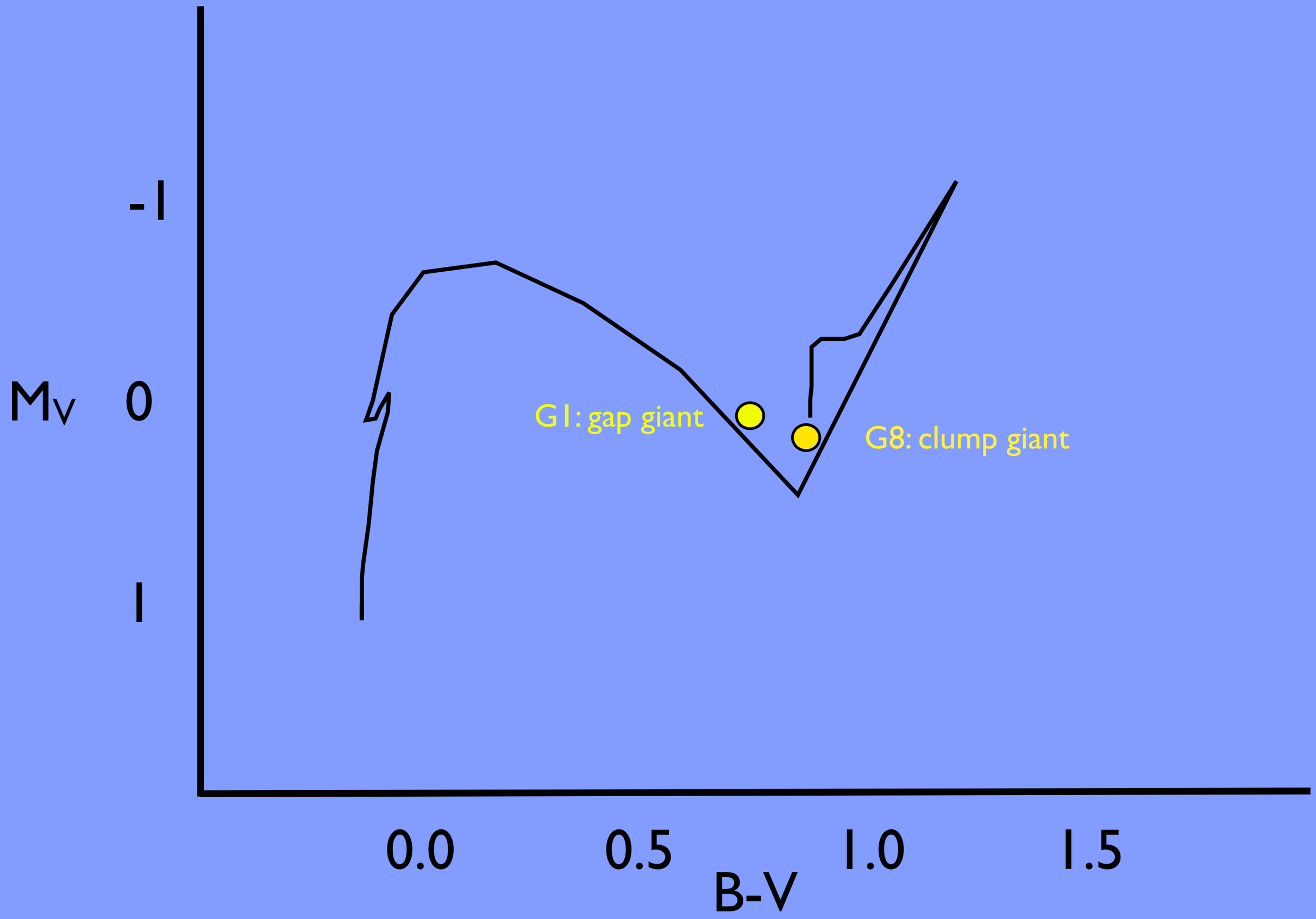
-1
M_V 0
1
G1: gap giant
G8: clump giant
0.0
0.5
1.0
1.5
B-V

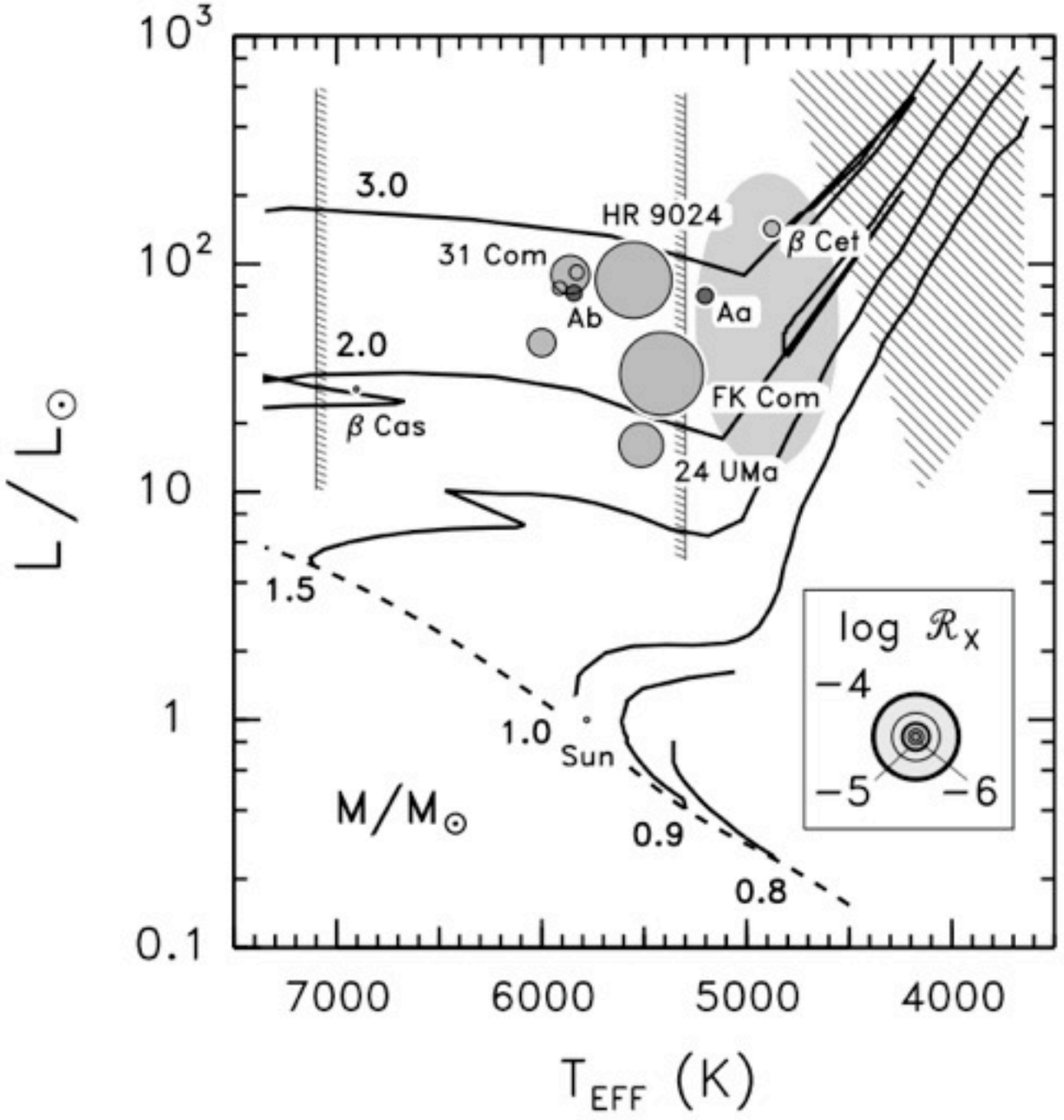

FIG. 1.—H-R diagram for stars of the program. Size of each circle depicts normalized X-ray flux ($\mathcal{R}_X \equiv f_X/f_{bol}$) according to legend at lower right. Key objects are labeled explicitly: "Aa" and "Ab" refer to Capella G8 and G0, respectively. Solid curves are evolutionary tracks from Schaller et al. (1992); zero-age main sequence is dashed. Vertical hatched lines delimit the Hertzsprung gap, shaded oval indicates the postflash "clump," and hatched area to right outlines the "noncoronal" zone where stellar soft X-ray detections are rare.

Ayres et al. 1998, ApJ, 496, 428

Capella HRC−S/LETG coadded

[ct/0.0125Å]

1000

100

5

10

15

20

C N O Ne Mg Si S Fe

[ct/0.0125Å]

1000

100

20 40 60 80 100 120 140 160

[Å]

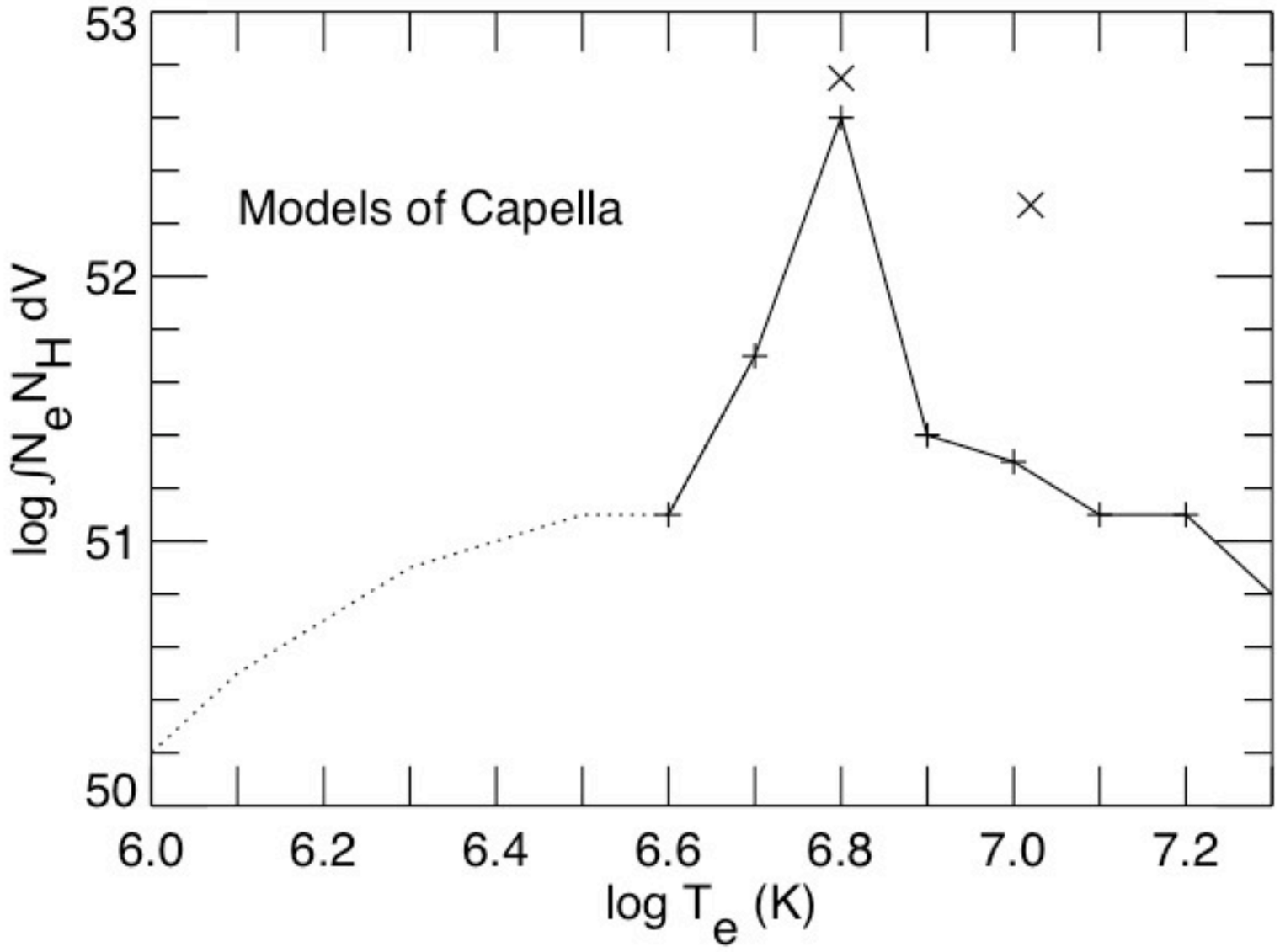

FIG. 3.—EM distribution derived from the EUV Fe line intensities listed in Table 1 for the Capella data of 1996 March 3–7, shown as a solid curve extended to lower temperature by a dotted curve. The model below log $T_e = 6.6$ (i.e., the *dott* a significant effect on fits to the *ASCA* spectrum bu ng Fe IX λ171.07 line. Plus signs mark the temperatu ous-temperature (Cont-T) models, as described in t e 2-T model that best fits the *ASCA* SIS0 + SIS1 s olumn of Table 2).

Brickhouse et al., 2000
Dupree et al., 1993
Ness et al., 2003
Argiroffi et al., 2003
Gu et al., 2006

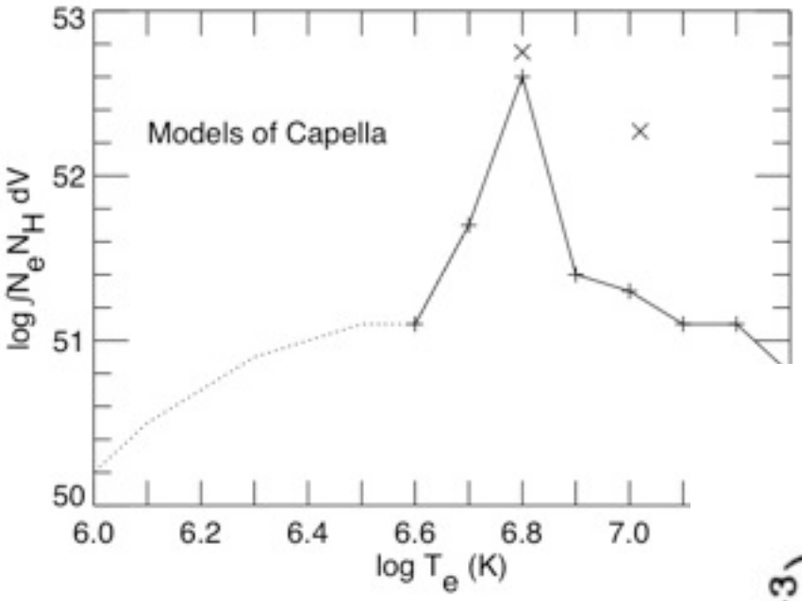

FIG. 3.—EM distribution derived from the EUV Fe line
listed in Table 1 for the Capella data of 1996 March 3–7, shown
curve extended to lower temperature by a dotted curve. The m
log $T_e = 6.6$ (i.e., the *dotted curve*) does not have a significant ef
to the *ASCA* spectrum but is required by the strong Fe IX λ171.0
signs mark the temperatures used in the continuous-temperatur
models, as described in the text. Crosses mark the 2-T model th
the *ASCA* SIS0 + SIS1 spectra (see the seventh column of Table

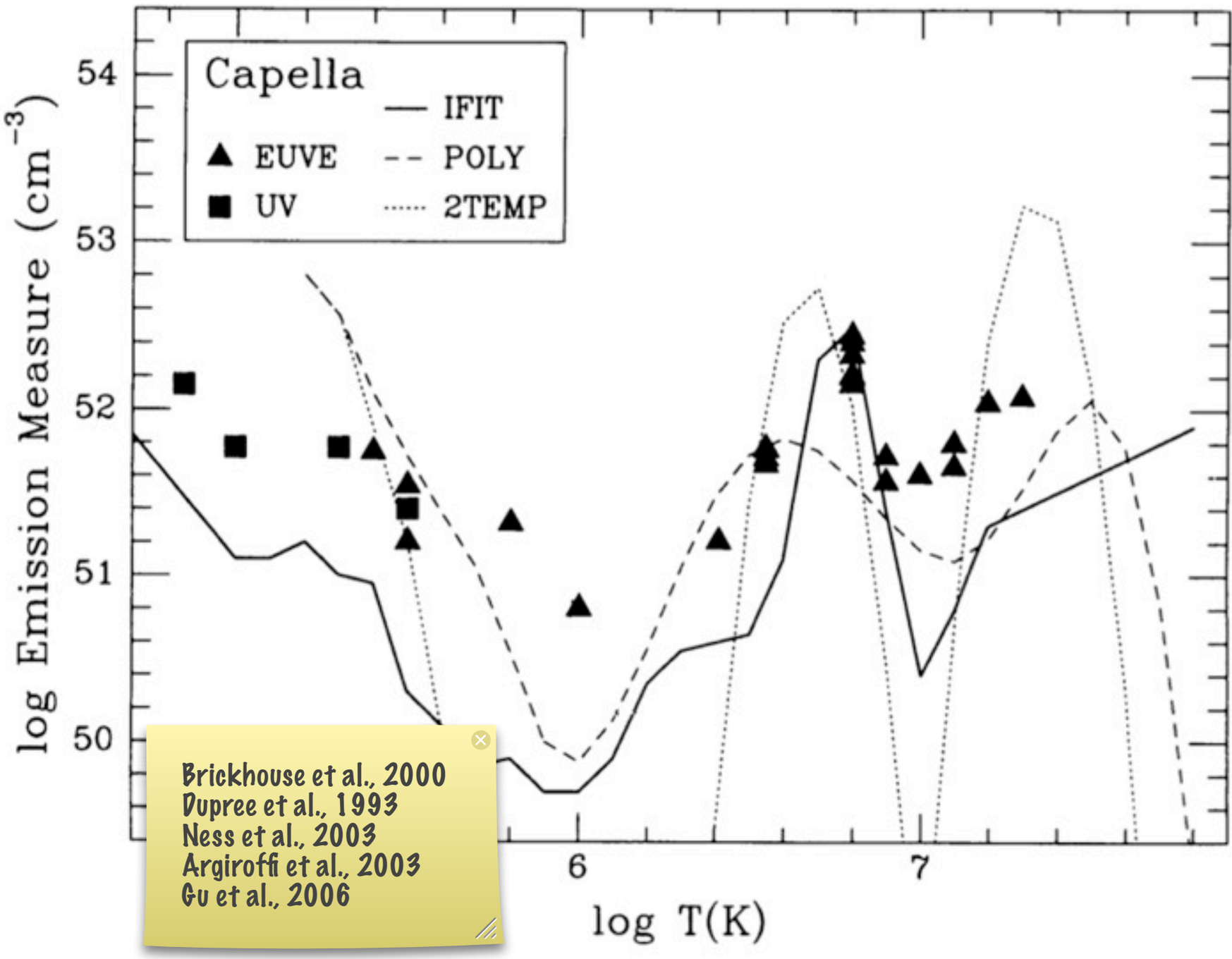

Brickhouse et al., 2000
Dupree et al., 1993
Ness et al., 2003
Argiroffi et al., 2003
Gu et al., 2006

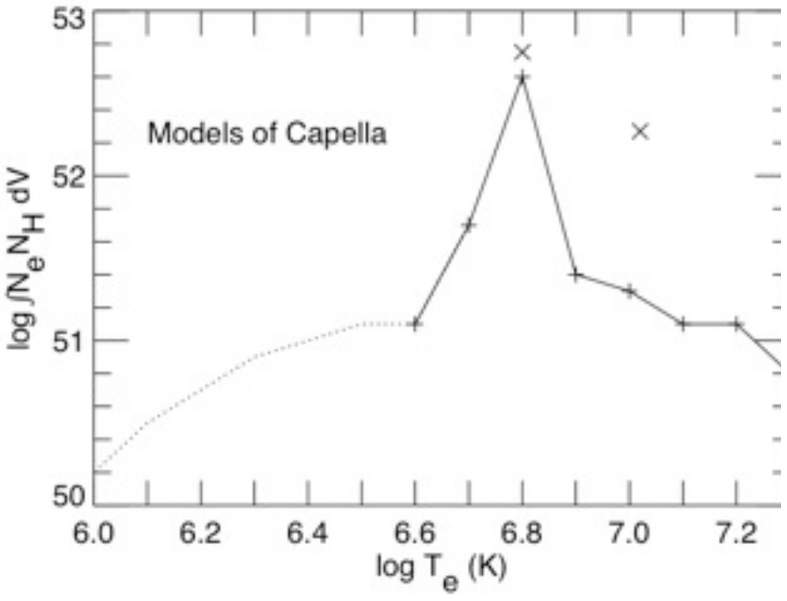

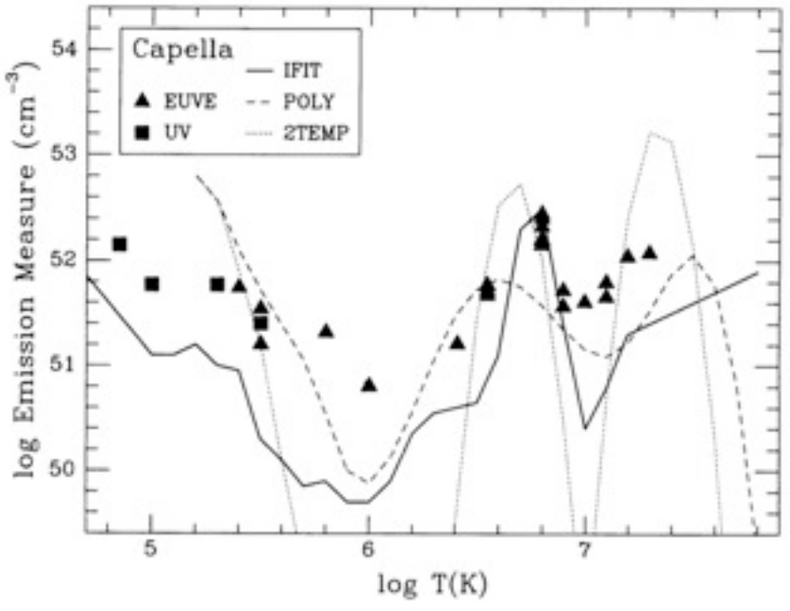

FIG. 3.—EM distribution derived from the EUV Fe line intensities listed in Table 1 for the Capella data of 1996 March 3–7, shown as a solid curve extended to lower temperature by a dotted curve. The model below log $T_e = 6.6$ (i.e., the *dotted curve*) does not have a significant effect on fits to the *ASCA* spectrum but is required by the strong Fe IX λ171.07 line. Plus signs mark the temperatures used in the continuous-temperature (Cont-T) models, as described in the text. Crosses mark the 2-T model that best fits the *ASCA* SIS0 + SIS1 spectra (see the seventh column of Table 2).

Brickhouse et al., 2000
Dupree et al., 1993
Ness et al., 2003
Argiroffi et al., 2003
Gu et al., 2006

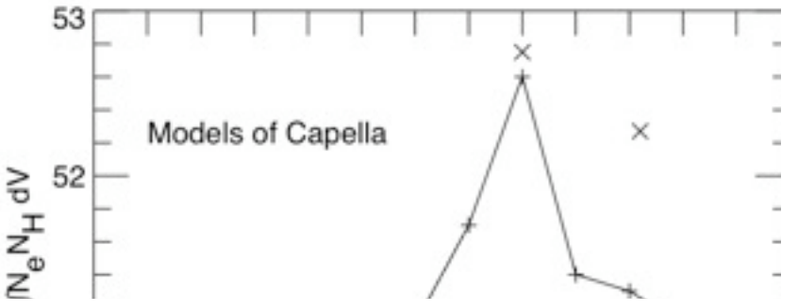

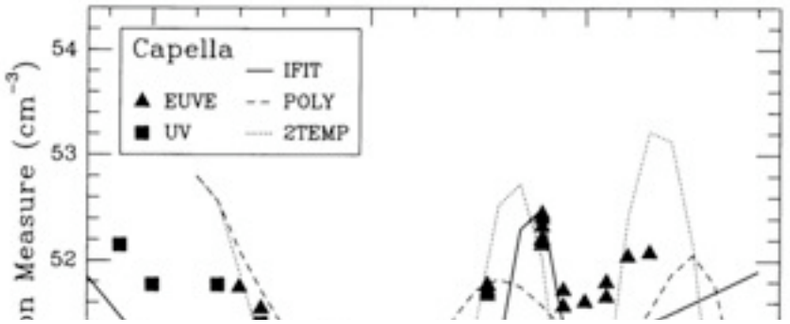

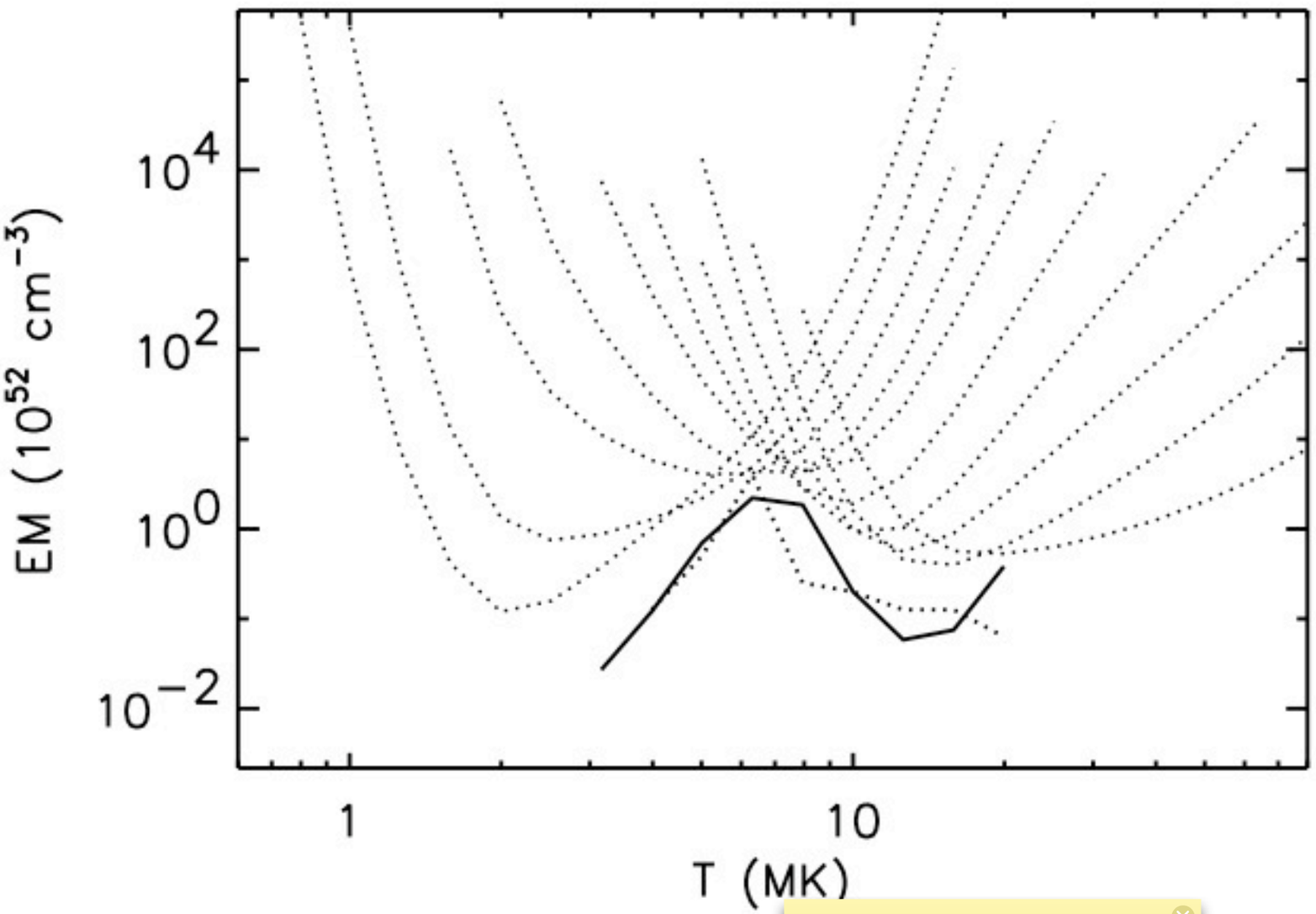

FIG. 7.—Best-fit emission measure distribu lines in ionization stages Fe XV to Fe XXIV (*solid line* khouse et al. (2000) is also shown (*lower dotted l* ission measure curves (*upper dotted lines*) are shown

Brickhouse et al., 2000
Dupree et al., 1993
Ness et al., 2003
Argiroffi et al., 2003
Gu et al., 2006

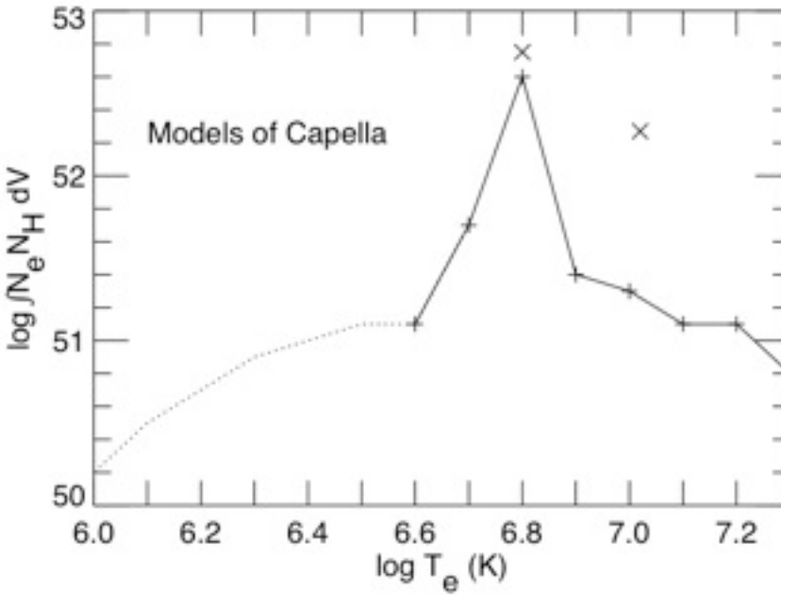

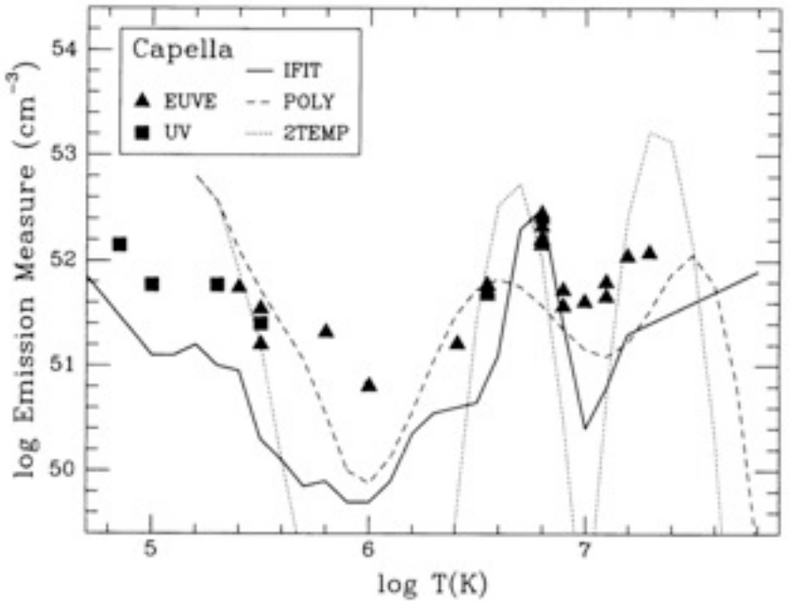

FIG. 3.—EM distribution derived from the EUV Fe line intensities listed in Table 1 for the Capella data of 1996 March 3–7, shown as a solid curve extended to lower temperature by a dotted curve. The model below log $T_e = 6.6$ (i.e., the *dotted curve*) does not have a significant effect on fits to the *ASCA* spectrum but is required by the strong Fe IX λ171.07 line. Plus signs mark the temperatures used in the continuous-temperature (Cont-T) models, as described in the text. Crosses mark the 2-T model that best fits the *ASCA* SIS0 + SIS1 spectra (see the seventh column of Table 2).

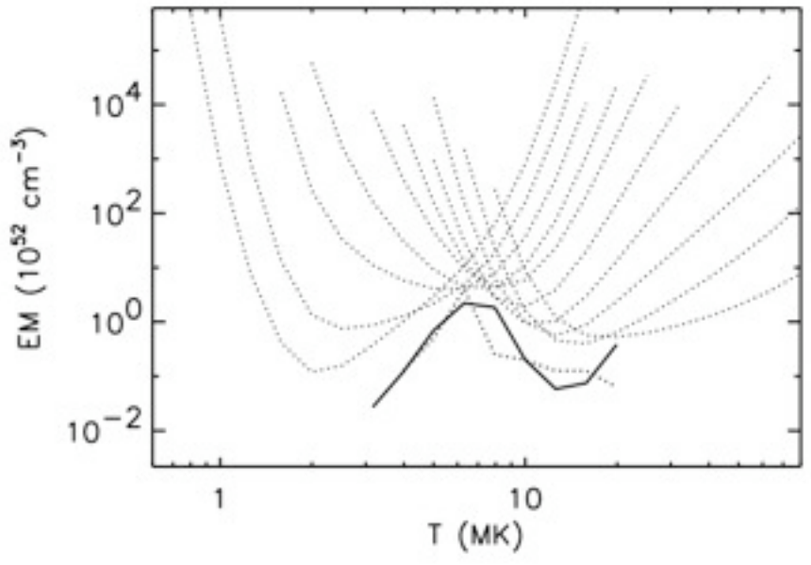

FIG. 7.—Best-fit emission measure distribution derived from iron lines in ionization stages Fe XV to Fe XXIV (*solid line*). The result from Brickhouse et al. (2000) is also shown (*lower dotted line*). Individual line emission measure curves (*upper dotted lines*) are shown for the lines in Table 6.

Brickhouse et al., 2000
Dupree et al., 1993
Ness et al., 2003
Argiroffi et al., 2003
Gu et al., 2006

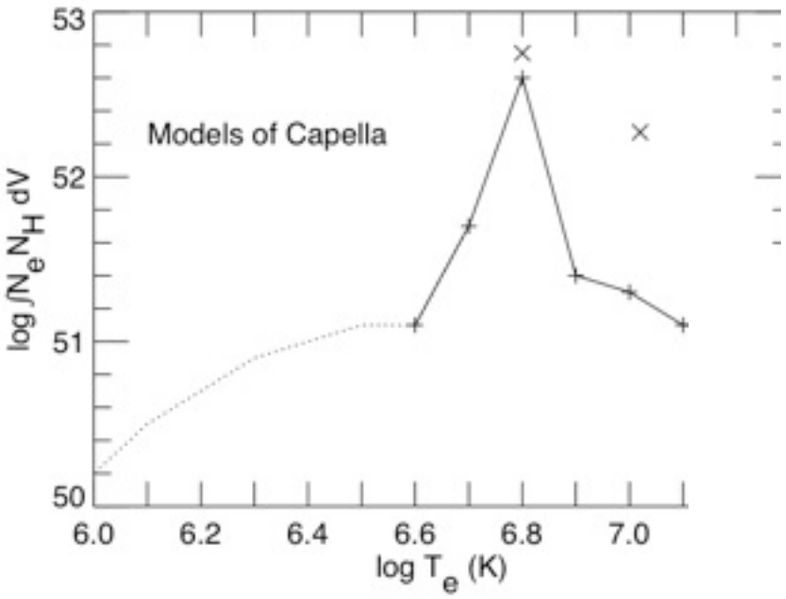

FIG. 3.—EM distribution derived from the EUV Fe line listed in Table 1 for the Capella data of 1996 March 3–7, shown curve extended to lower temperature by a dotted curve. The m log $T_e = 6.6$ (i.e., the *dotted curve*) does not have a significant ef to the *ASCA* spectrum but is required by the strong Fe IX λ171.0 signs mark the temperatures used in the continuous-temperatur models, as described in the text. Crosses mark the 2-T model th the *ASCA* SIS0 + SIS1 spectra (see the seventh column of Table

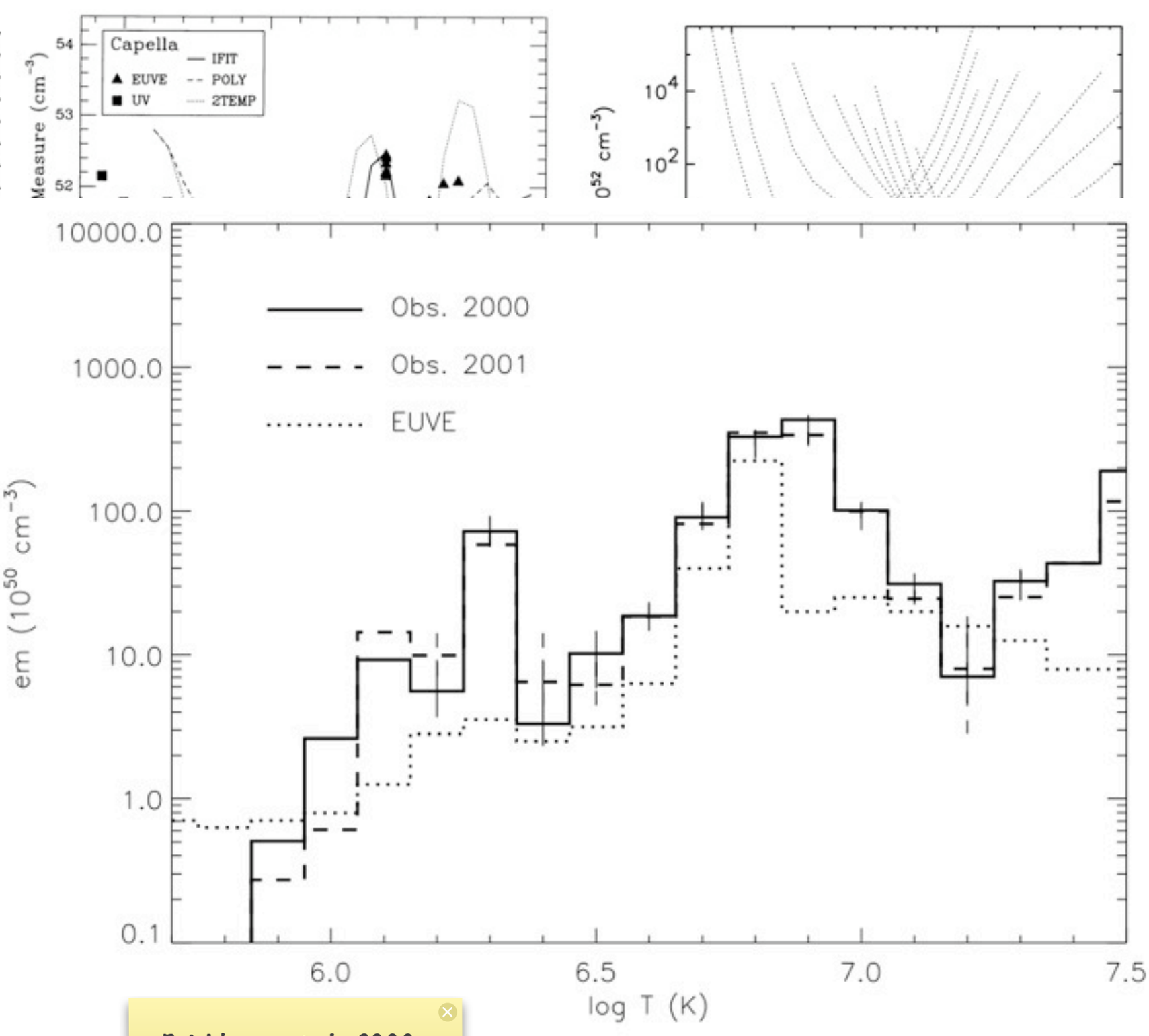

Fig. 11. sure distributions (solid for observation taken in or observation taken in 2001) and EUVE emissio ion (dotted) obtained by Dupree et al. (2003).

Brickhouse et al., 2000
Dupree et al., 1993
Ness et al., 2003
Argiroffi et al., 2003
Gu et al., 2006

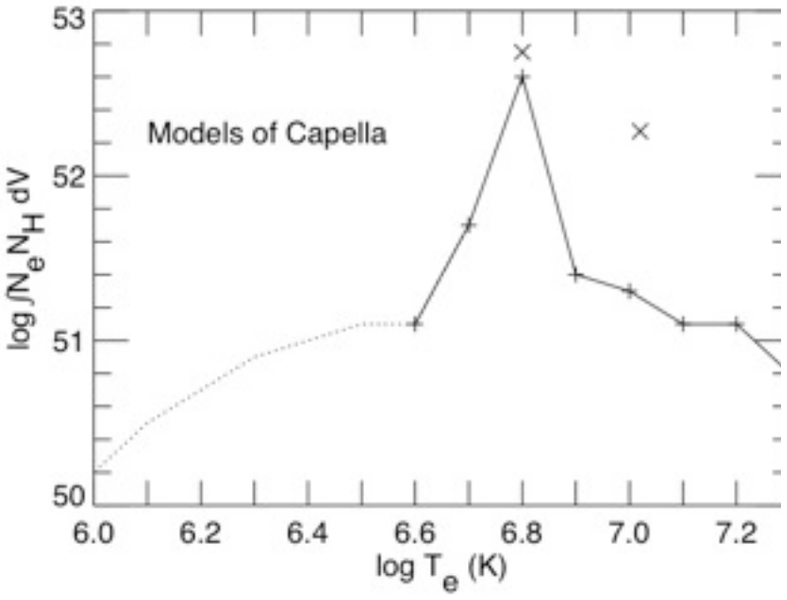

FIG. 3.—EM distribution derived from the EUV Fe line intensities listed in Table 1 for the Capella data of 1996 March 3–7, shown as a solid curve extended to lower temperature by a dotted curve. The model below log $T_e = 6.6$ (i.e., the *dotted curve*) does not have a significant effect on fits to the *ASCA* spectrum but is required by the strong Fe IX λ171.07 line. Plus signs mark the temperatures used in the continuous-temperature (Cont-T) models, as described in the text. Crosses mark the 2-T model that best fits the *ASCA* SIS0 + SIS1 spectra (see the seventh column of Table 2).

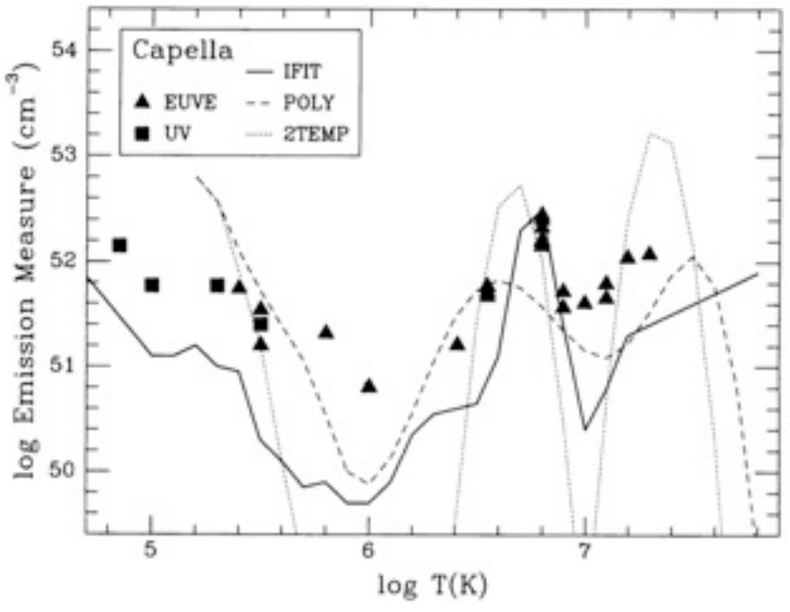

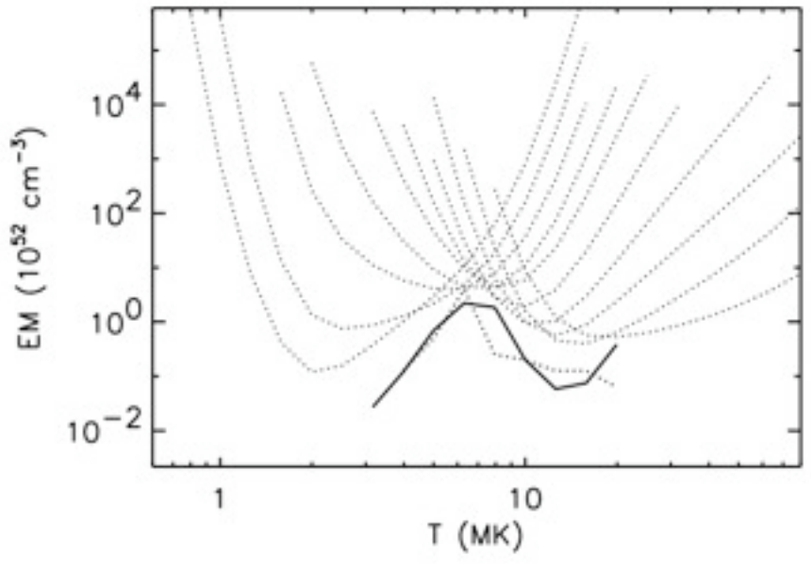

FIG. 7.—Best-fit emission measure distribution derived from iron lines in ionization stages Fe XV to Fe XXIV (*solid line*). The result from Brickhouse et al. (2000) is also shown (*lower dotted line*). Individual line emission measure curves (*upper dotted lines*) are shown for the lines in Table 6.

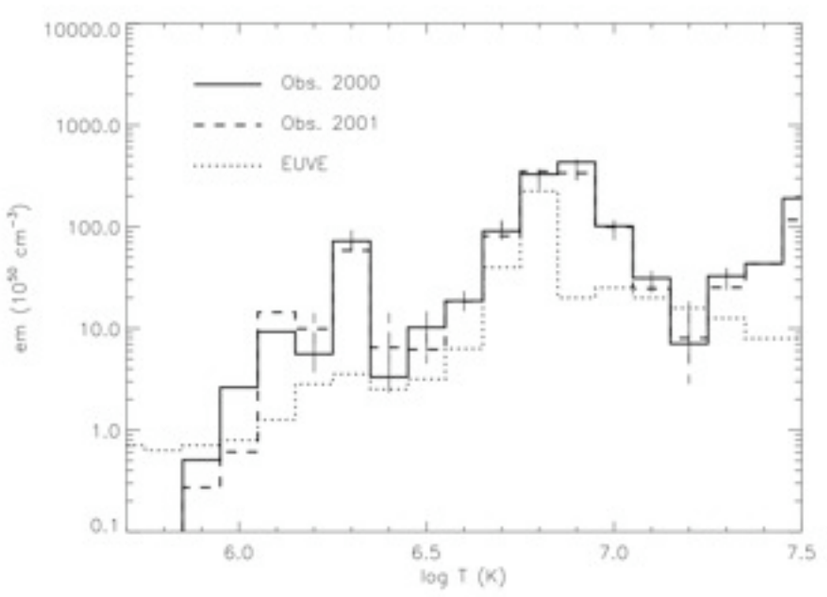

Fig. 11. Our emission measure distributions (solid for observation taken in 2000 and dashed for observation taken in 2001) and EUVE emission measure distribution (dotted) obtained by Dupree et al. (2003).

Brickhouse et al., 2000
Dupree et al., 1993
Ness et al., 2003
Argiroffi et al., 2003
Gu et al., 2006

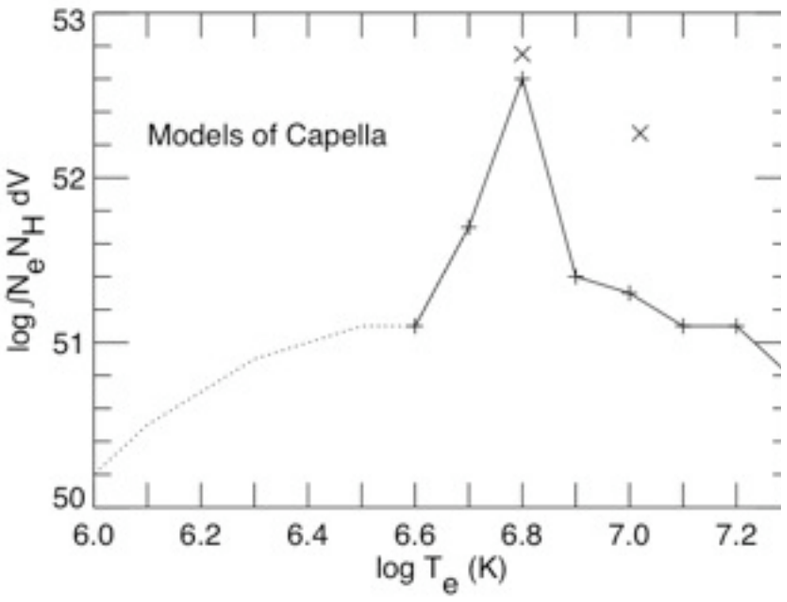

FIG. 3.—EM distribution derived from the EUV Fe line intensities listed in Table 1 for the Capella data of 1996 March 3–7, shown as a solid curve extended to lower temperature by a dotted curve. The model below $\log T_e = 6.6$ (i.e., the *dotted curve*) does not have a significant effect on fits to the *ASCA* spectrum but is required by the strong Fe IX λ171.07 line. Plus signs mark the temperatures used in the continuous-temperature (Cont-T) models, as described in the text. Crosses mark the 2-T model that best fits the *ASCA* SIS0 + SIS1 spectra (see the seventh column of Table 2).

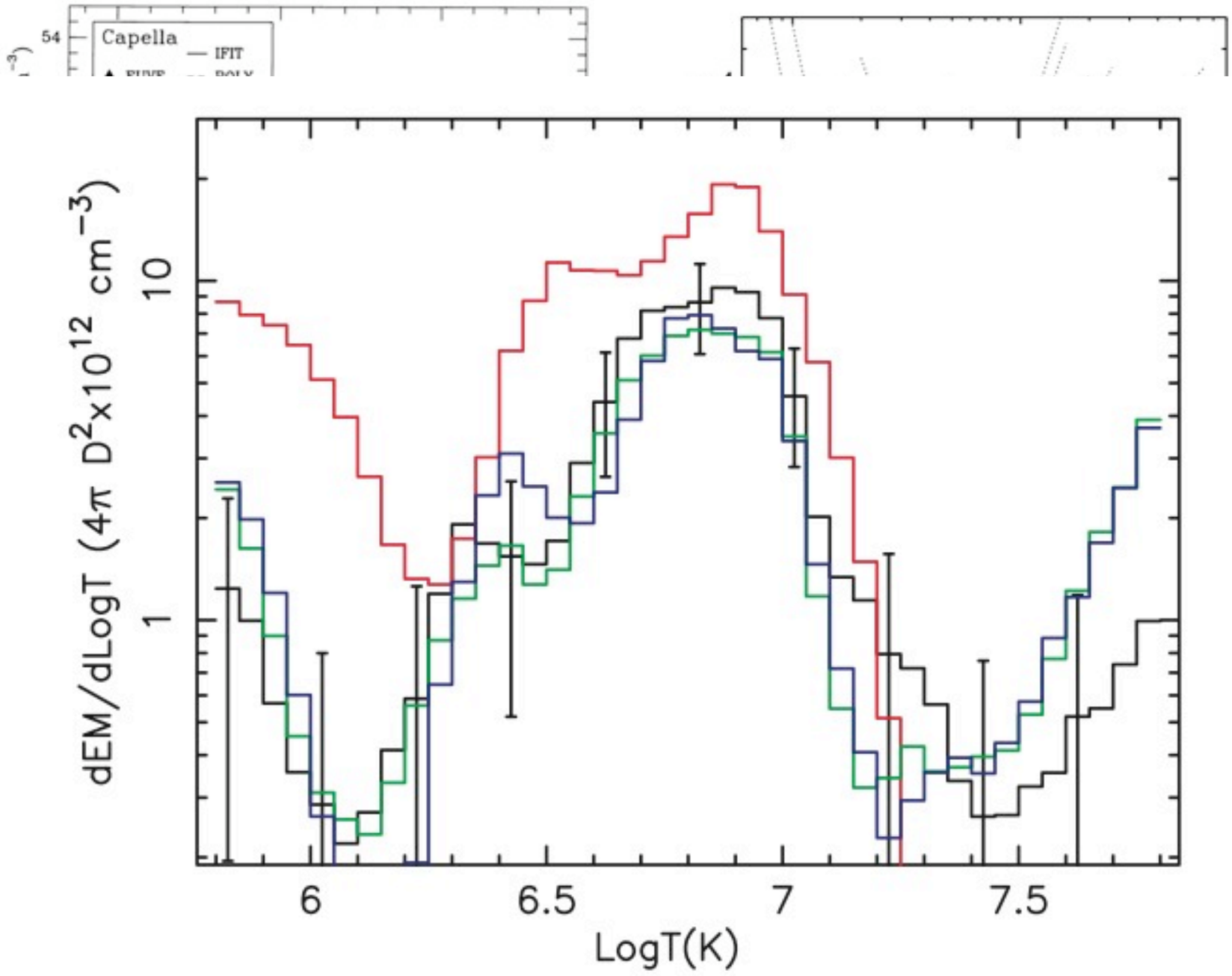

FIG. 6.—Reconstructed DEM for the Capella corona. The black histogram with error bars is the reconstruction from the joint fit of HETGS and RGS data, the green histog… from the RGS data alone, the blue histogram is the recons… data with the L-shell emission of intermediate-Z eleme… luded, and the red histogram is the reconstruction from t… e error bars represent 1 σ statistical uncertainties and ar… make the figure less cluttered.

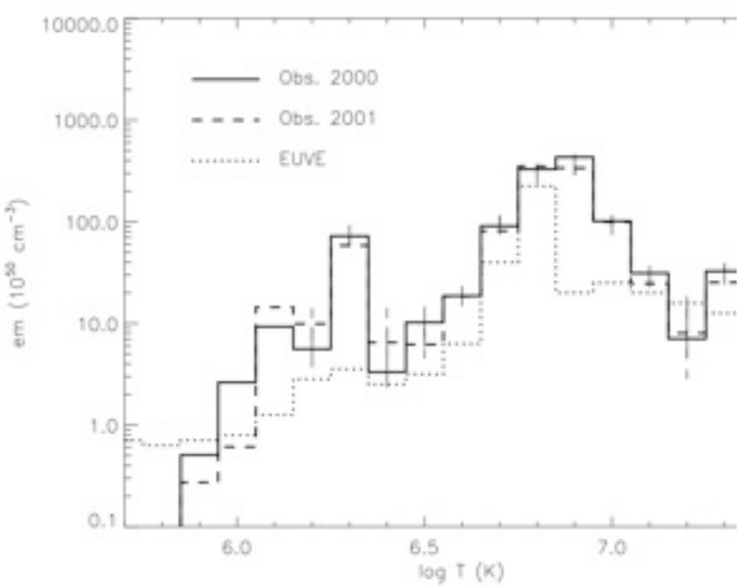

Fig. 11. Our emission measure distributions (solid for obser… taken in 2000 and dashed for observation taken in 2001) and … emission measure distribution (dotted) obtained by Dupree … (2003).

Brickhouse et al., 2000
Dupree et al., 1993
Ness et al., 2003
Argiroffi et al., 2003
Gu et al., 2006

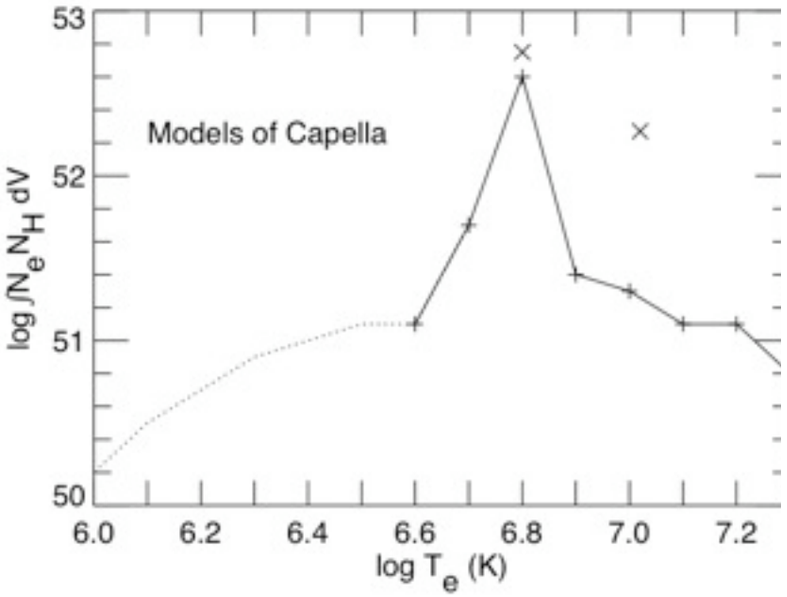

FIG. 3.—EM distribution derived from the EUV Fe line intensities listed in Table 1 for the Capella data of 1996 March 3–7, shown as a solid curve extended to lower temperature by a dotted curve. The model below log $T_e = 6.6$ (i.e., the *dotted curve*) does not have a significant effect on fits to the *ASCA* spectrum but is required by the strong Fe IX λ171.07 line. Plus signs mark the temperatures used in the continuous-temperature (Cont-T) models, as described in the text. Crosses mark the 2-T model that best fits the *ASCA* SIS0 + SIS1 spectra (see the seventh column of Table 2).

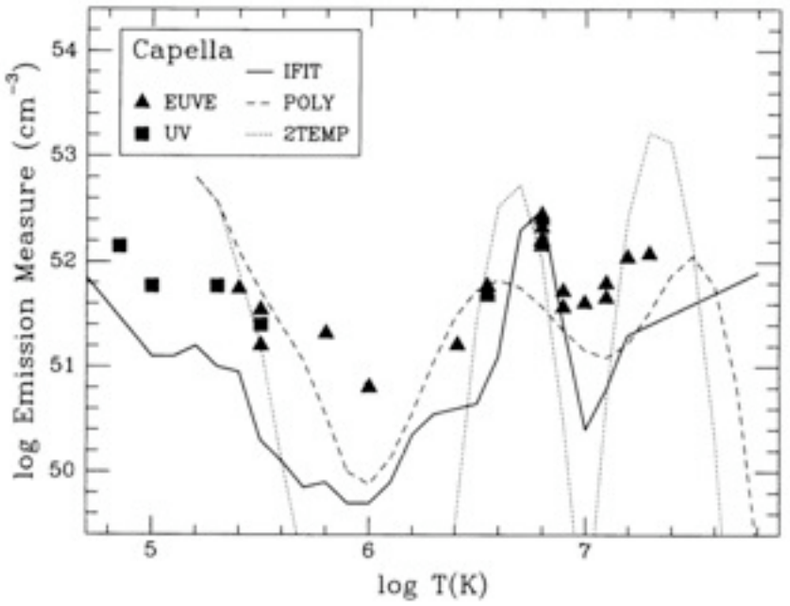

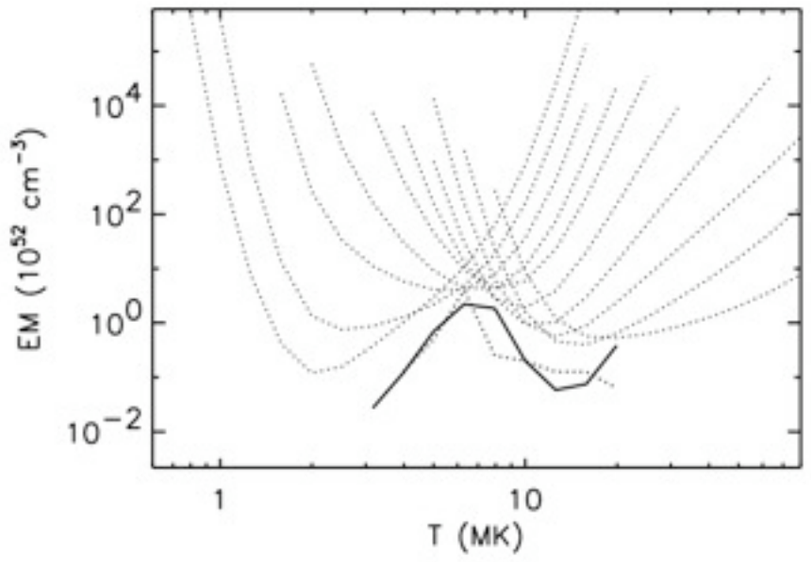

FIG. 7.—Best-fit emission measure distribution derived from iron lines in ionization stages Fe XV to Fe XXIV (*solid line*). The result from Brickhouse et al. (2000) is also shown (*lower dotted line*). Individual line emission measure curves (*upper dotted lines*) are shown for the lines in Table 6.

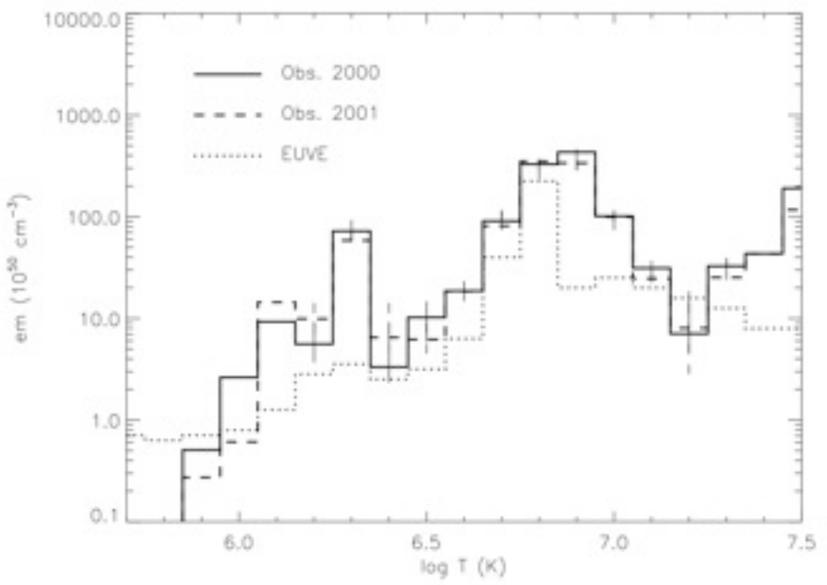

Fig. 11. Our emission measure distributions (solid for observation taken in 2000 and dashed for observation taken in 2001) and EUVE emission measure distribution (dotted) obtained by Dupree et al. (2003).

G1 or G8?
Or both?

Brickhouse et al., 2000
Dupree et al., 1993
Ness et al., 2003
Argiroffi et al., 2003
Gu et al., 2006

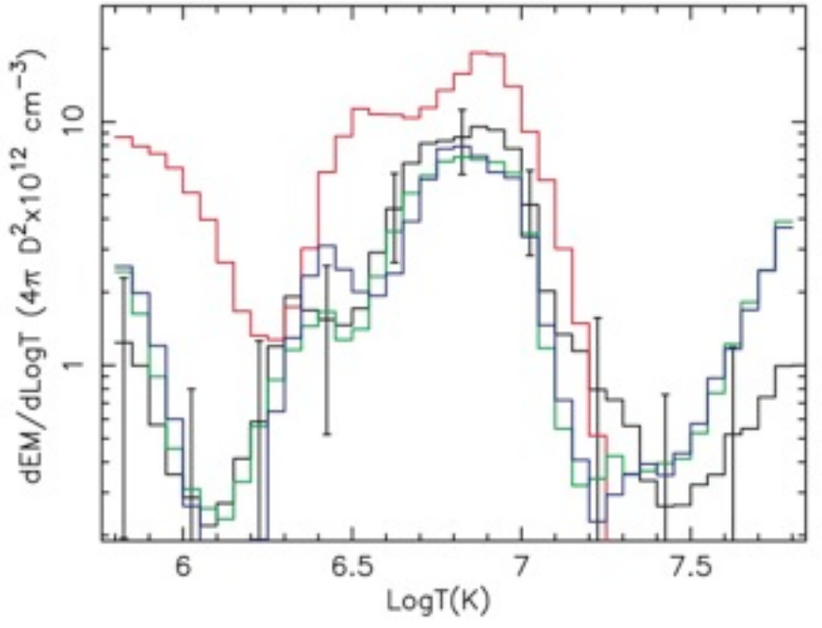

FIG. 6.—Reconstructed DEM for the Capella corona. The black histogram with error bars is the reconstruction from the joint fit of HETGS and RGS data, the green histogram is the reconstruction from the RGS data alone, the blue histogram is the reconstruction from the RGS data with the L-shell emission of intermediate-Z elements (Si, S, Ar, and Ca) excluded, and the red histogram is the reconstruction from the HETGS data alone. The error bars represent 1 σ statistical uncertainties and are plotted every fifth bin to make the figure less cluttered.

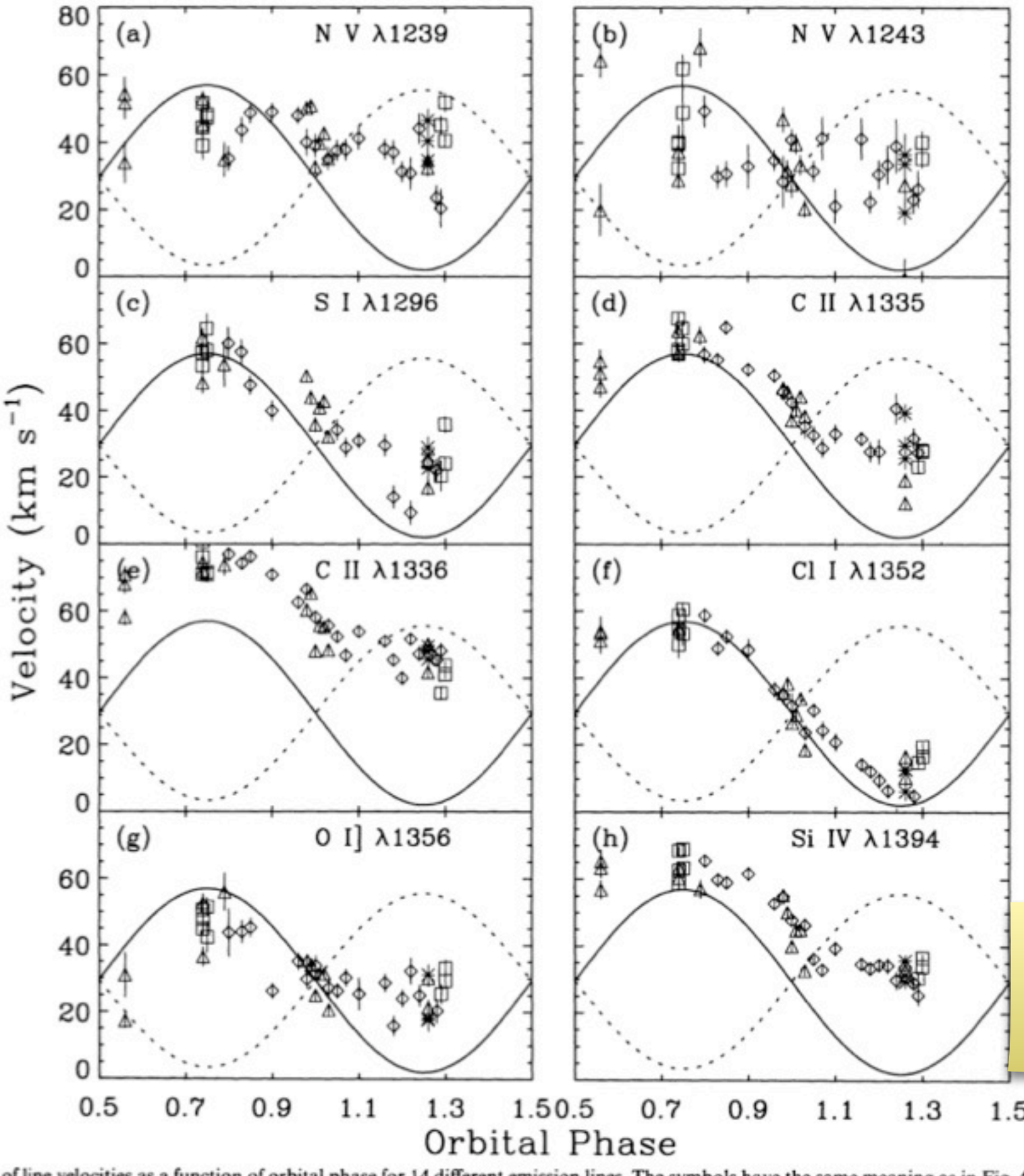

Wood & Ayres 1995
Young et al., 2001
Ishibashi et al., 2006

FIG. 5.—Plots of line velocities as a function of orbital phase for 14 different emission lines. The symbols have the same meaning as in Fig. 4. Solid lines represent the rest frame of the G1 star, and dotted lines represent the rest frame of the G8 star. Measurements made on spectra with exposure times of 30 minutes or less were omitted for clarity (except for Si III] λ1892 and C III] λ1909).

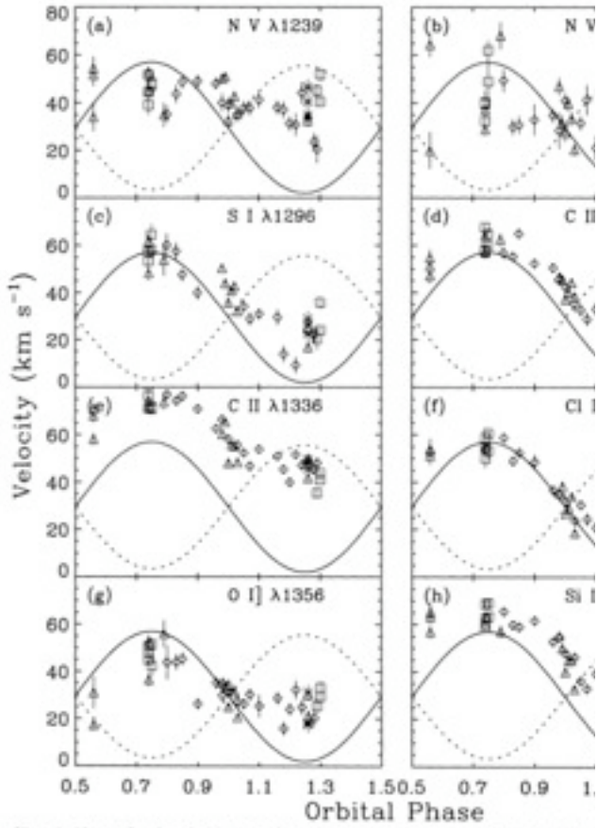

FIG. 5.—Plots of line velocities as a function of orbital phase for 14 different emission lines. The symbols have the sa
the rest frame of the G1 star, and dotted lines represent the rest frame of the G8 star. Measurements made on spectra w
omitted for clarity (except for Si III] λ1892 and C III] λ1909).

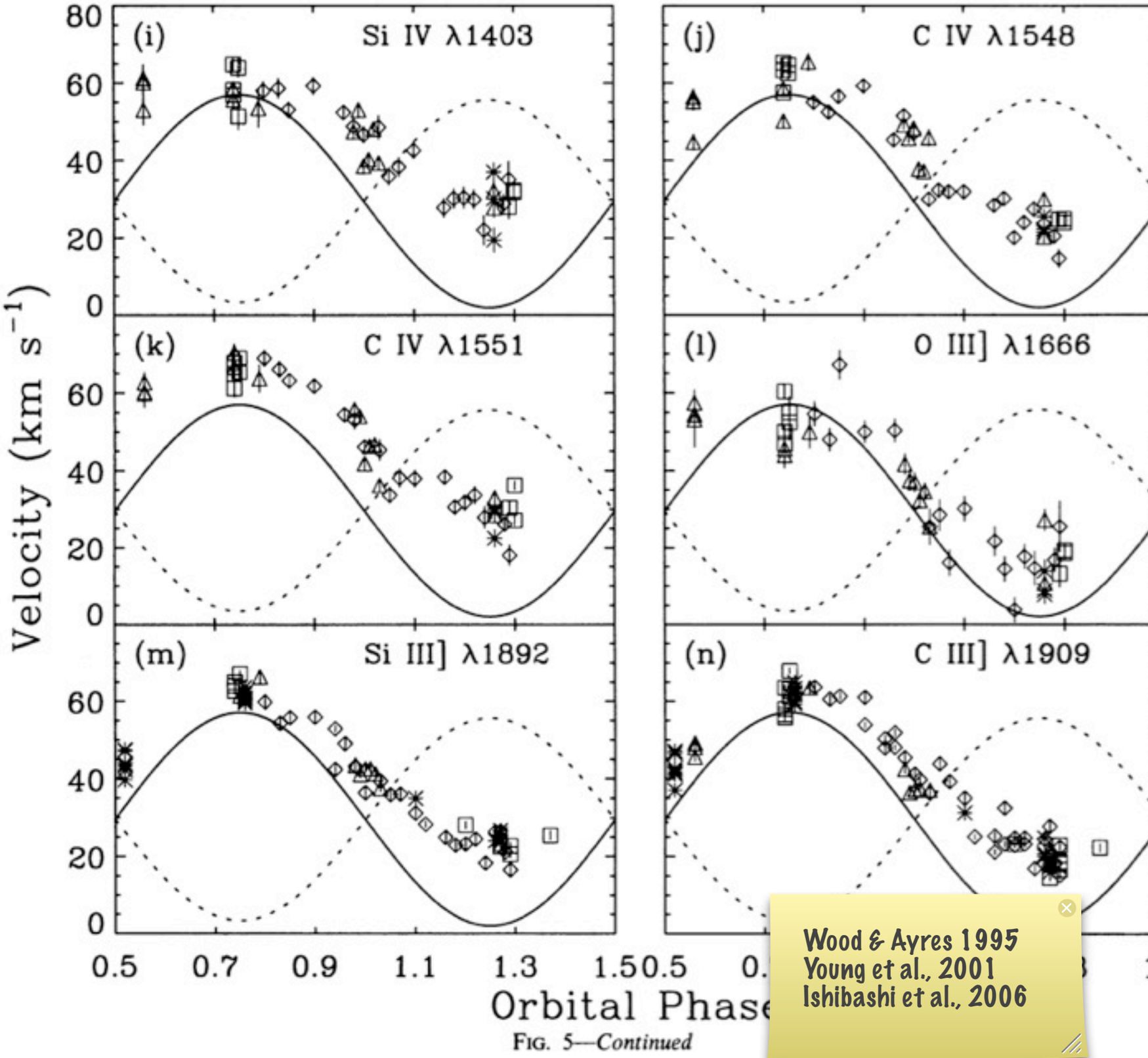

FIG. 5—*Continued*

Wood & Ayres 1995
Young et al., 2001
Ishibashi et al., 2006

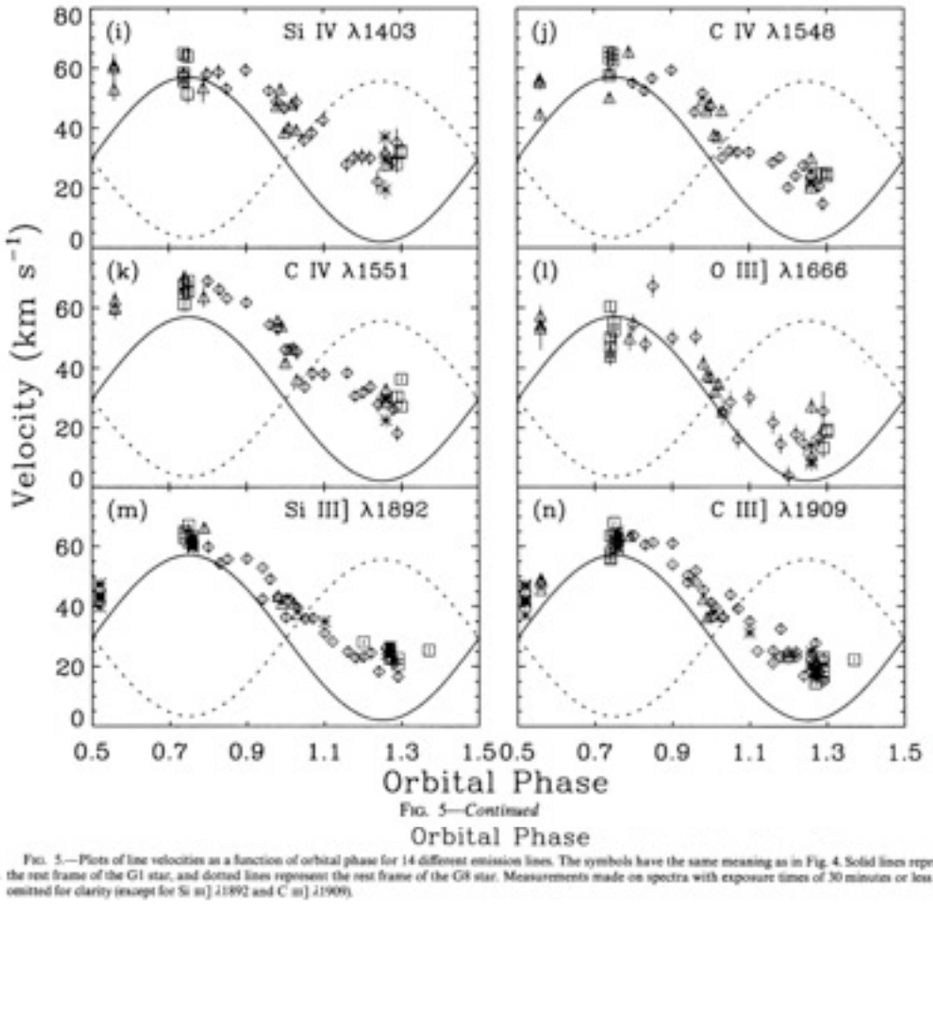

FIG. 5—*Continued*

Orbital Phase

FIG. 5.—Plots of line velocities as a function of orbital phase for 14 different emission lines. The symbols have the same meaning as in Fig. 4. Solid lines represent the rest frame of the G1 star, and dotted lines represent the rest frame of the G8 star. Measurements made on spectra with exposure times of 30 minutes or less were omitted for clarity (except for Si III] λ1892 and C III] λ1909).

Wood & Ayres 1995
Young et al., 2001
Ishibashi et al., 2006

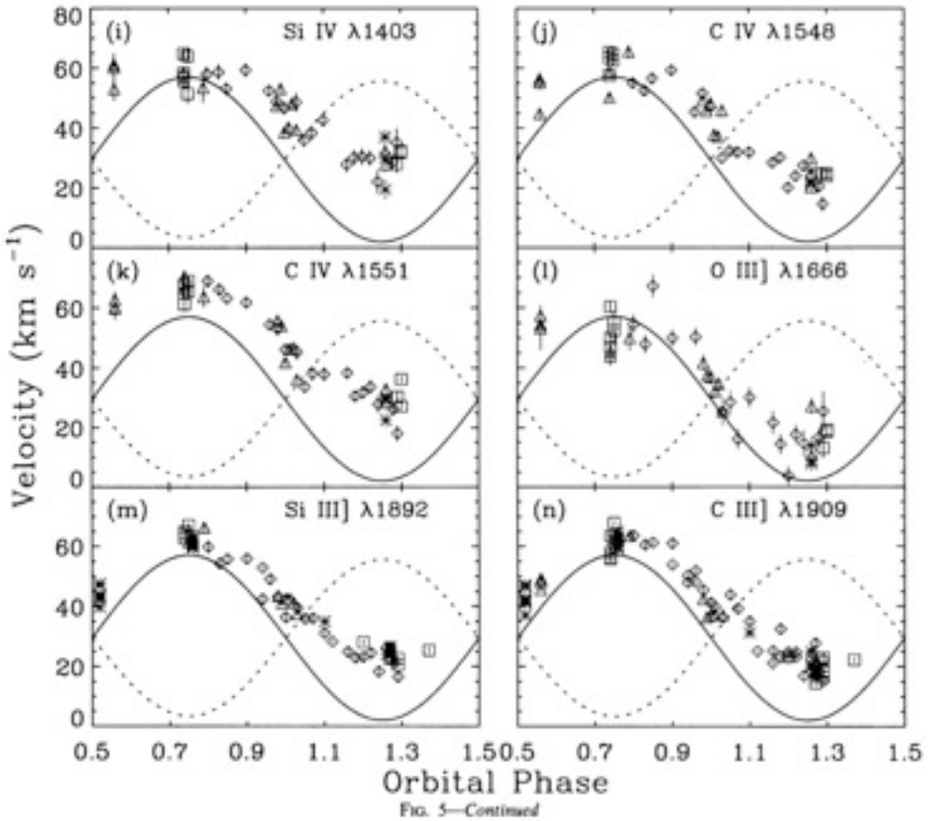

FIG. 5.—*Continued*

Orbital Phase

FIG. 5.—Plots of line velocities as a function of orbital phase for 14 different emission lines. The symbols have the same meaning as in Fig. 4. Solid lines represent the rest frame of the G1 star, and dotted lines represent the rest frame of the G8 star. Measurements made on spectra with exposure times of 30 minutes or less were omitted for clarity (except for Si III] λ1892 and C III] λ1909).

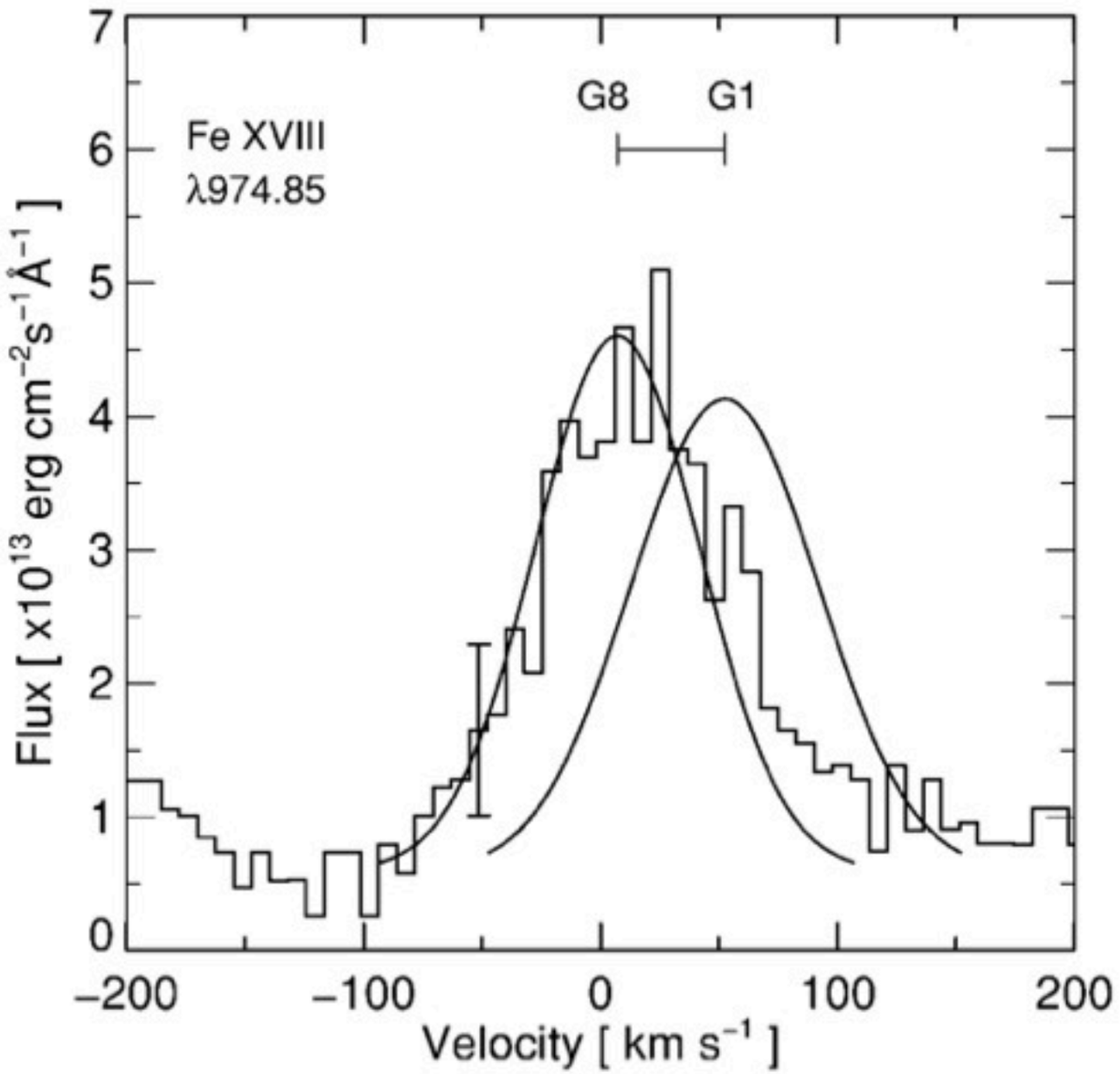

FIG. 3.—Fe XVIII λ974 profile from the SiC2A spectrum of the 2000 November 5 observation. The zero point of the velocity scale corresponds to the rest wavelength of the line, determined fro n at 977 Å. The expected velocities of the Capel with two model profiles centered at the two stars files show the appearance of the Fe XVIII line if the two stars, and thus they demonstrate the do G8 giant. The model profiles are broadened with the thermal width of line λ974 (79 km s^{-1}), the *FUSE* instrumental broadening (20 km s^{-1}), and the rotational broadenings of each star (3 km s^{-1} for the G8 giant and 36 km s^{-1} for the G1 giant). A 1 σ error bar is also shown.

Wood & Ayres 1995
Young et al., 2001
Ishibashi et al., 2006

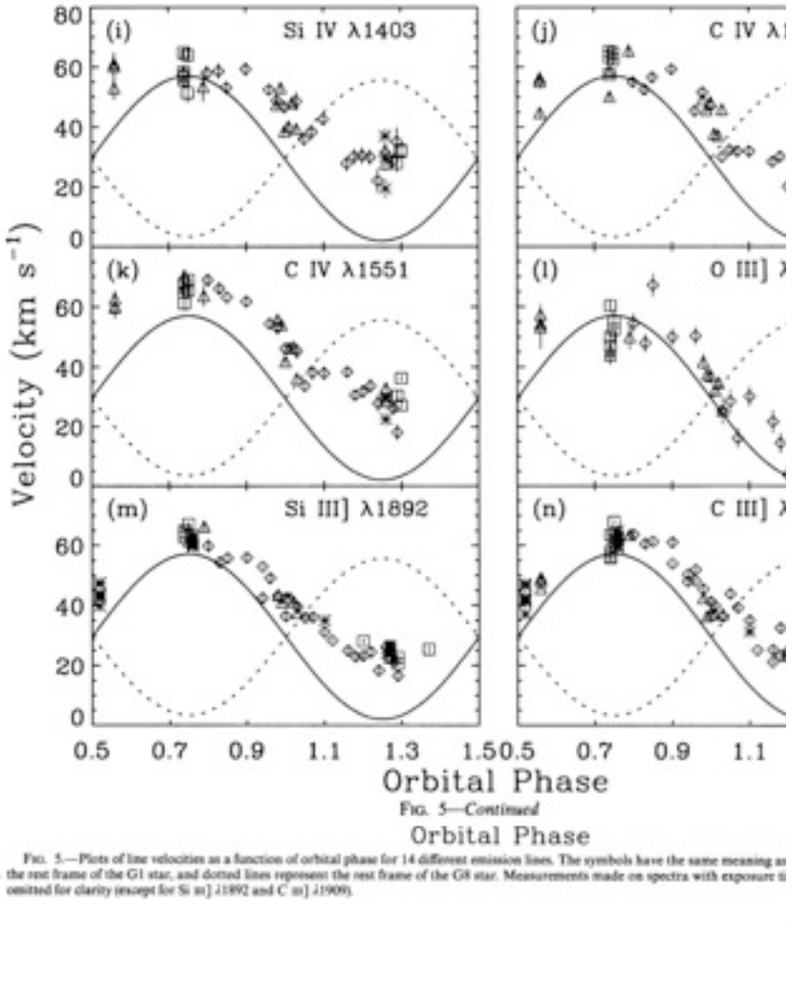

FIG. 5—*Continued*

Orbital Phase

FIG. 5.—Plots of line velocities as a function of orbital phase for 14 different emission lines. The symbols have the same meaning as the rest frame of the G1 star, and dotted lines represent the rest frame of the G8 star. Measurements made on spectra with exposure ti omitted for clarity (except for Si III] λ1892 and C III] λ1909).

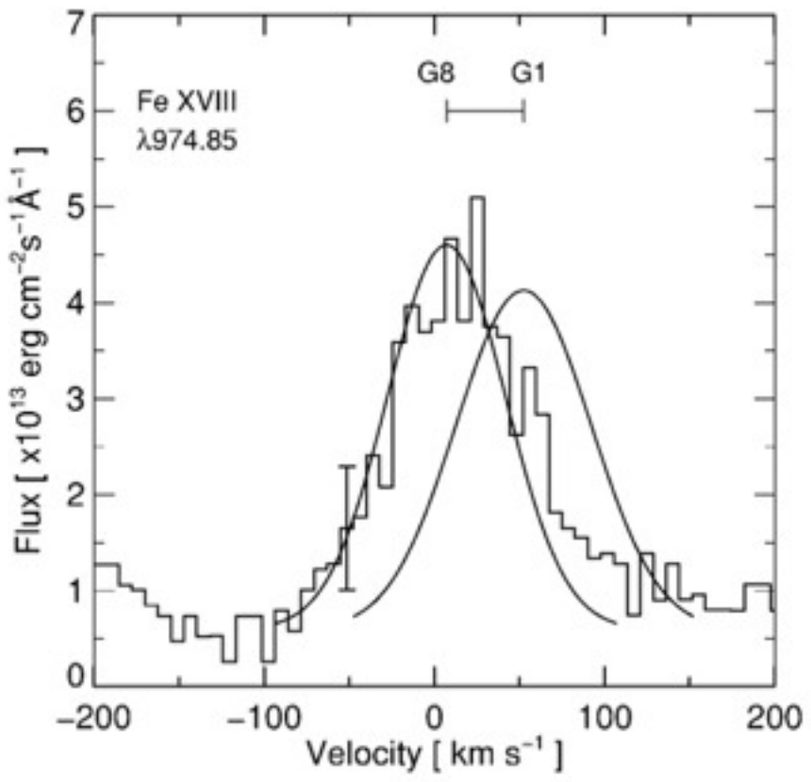

FIG. 3.—Fe XVIII λ974 profile from the SiC2A spectrum of the 2000 November 5 observation. The zero point of the velocity scale corresponds to the rest wavelength of the line, determined from interstellar C III absorption at 977 Å. The expected velocities of the Capella giants are shown, together with two model profiles centered at the two stars' velocities. These model profiles show the appearance of the Fe XVIII line if it originated solely in one of the two stars, and thus they demonstrate the dominant contribution from the G8 giant. The model profiles are broadened with the thermal width of line λ974 (79 km s^{-1}), the *FUSE* instrumental broadening (20 km s^{-1}), and the rotational broadenings of each star (3 km s^{-1} for the G8 giant and 36 km s^{-1} for the G1 giant). A 1 σ error bar is also shown.

Wood & Ayres 1995
Young et al., 2001
Ishibashi et al., 2006

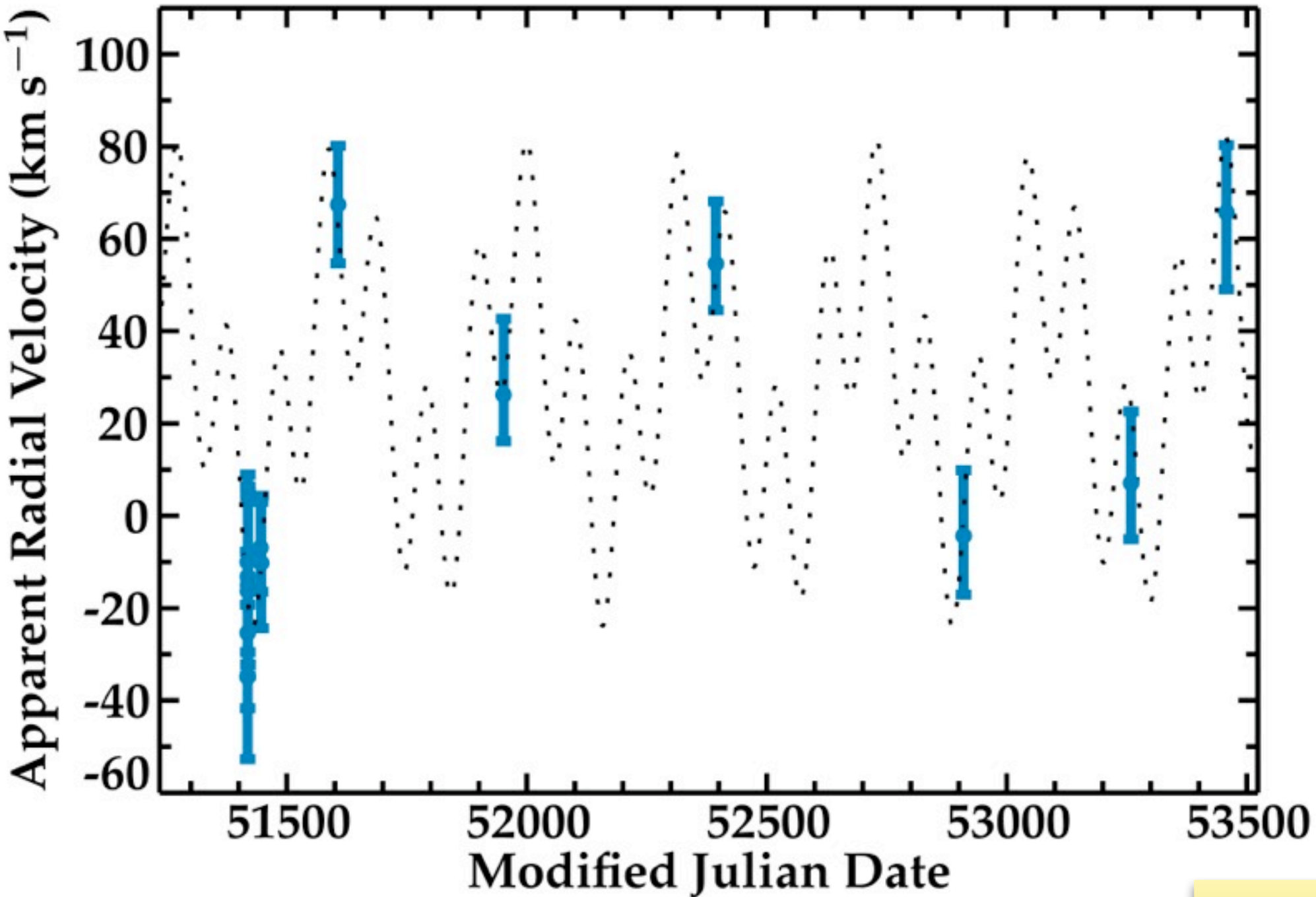

Wood & Ayres 1995
Young et al., 2001
Ishibashi et al., 2006

FIG. 1.—Apparent radial velocities of Capella measured with the C HETGS. The dotted line shows the calculated apparent radial motion of Capella Aa viewed from Earth (including the barycentric, orbital, and systemic motion of Capella Aa); 3 σ error bars are shown in the plot.

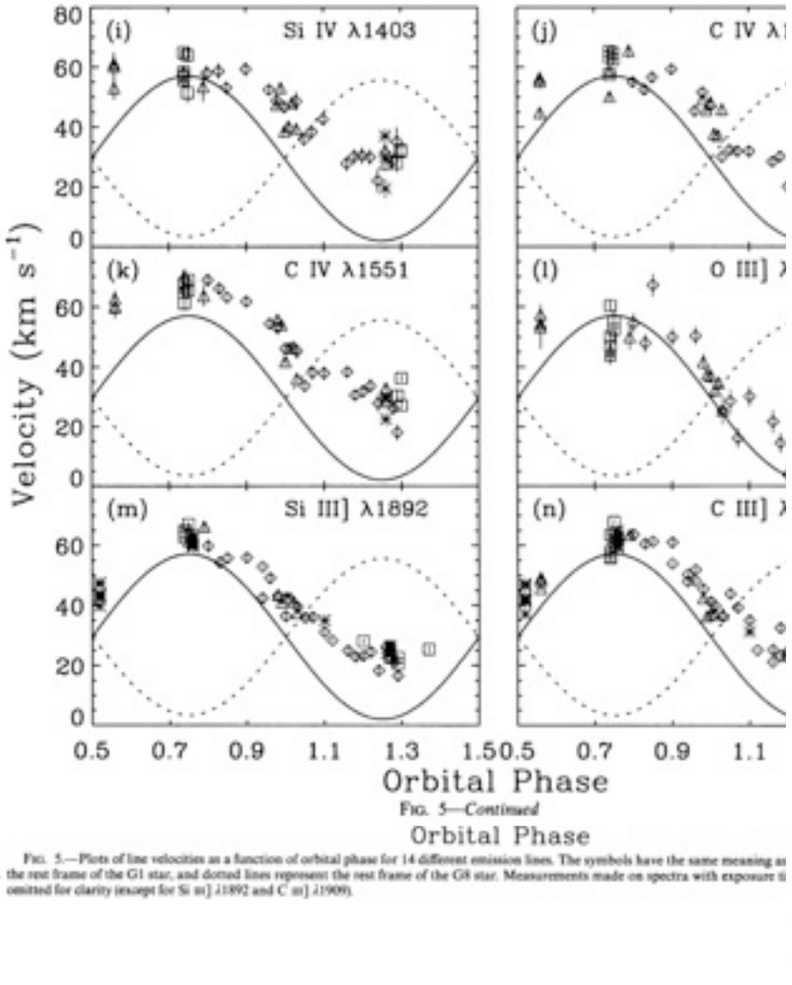

FIG. 5.—*Continued*

Orbital Phase

FIG. 5.—Plots of line velocities as a function of orbital phase for 14 different emission lines. The symbols have the same meaning as the rest frame of the G1 star, and dotted lines represent the rest frame of the G8 star. Measurements made on spectra with exposure ti omitted for clarity (except for Si III] λ1892 and C III] λ1909).

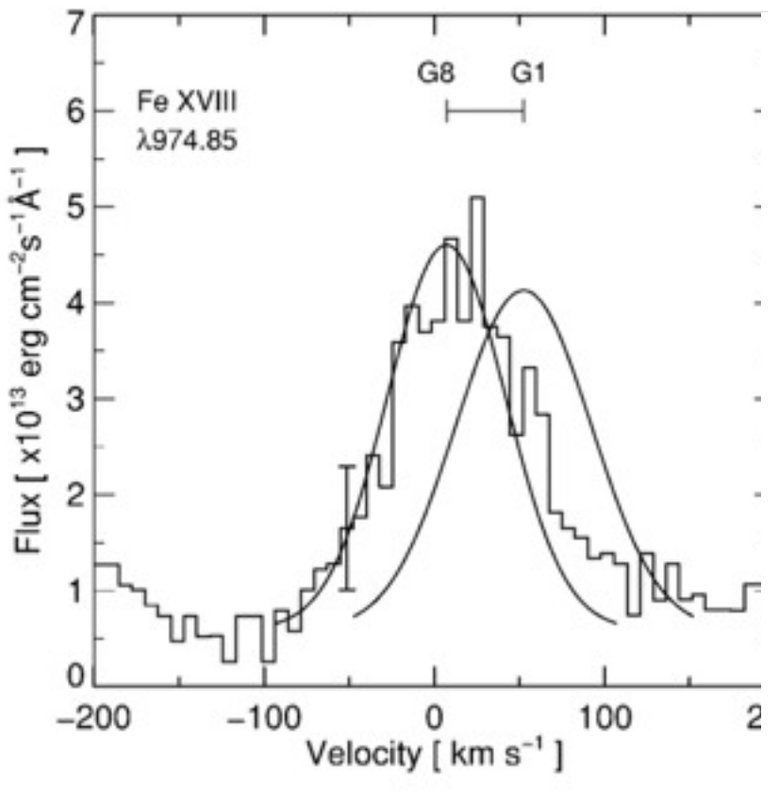

FIG. 3.—Fe XVIII λ974 profile from the SiC2A spectrum of the 2000 vember 5 observation. The zero point of the velocity scale corresponds t rest wavelength of the line, determined from interstellar C III absorption at 977 Å. The expected velocities of the Capella giants are shown, together with two model profiles centered at the two stars' velocities. These model profiles show the appearance of the Fe XVIII line if it originated solely in one of the two stars, and thus they demonstrate the dominant contribution from the G8 giant. The model profiles are broadened with the thermal width of line λ974 (79 km s^{-1}), the *FUSE* instrumental broadening (20 km s^{-1}), and the rotational broadenings of each star (3 km s^{-1} for the G8 giant and 36 km s^{-1} for the G1 giant). A 1 σ error bar is also shown.

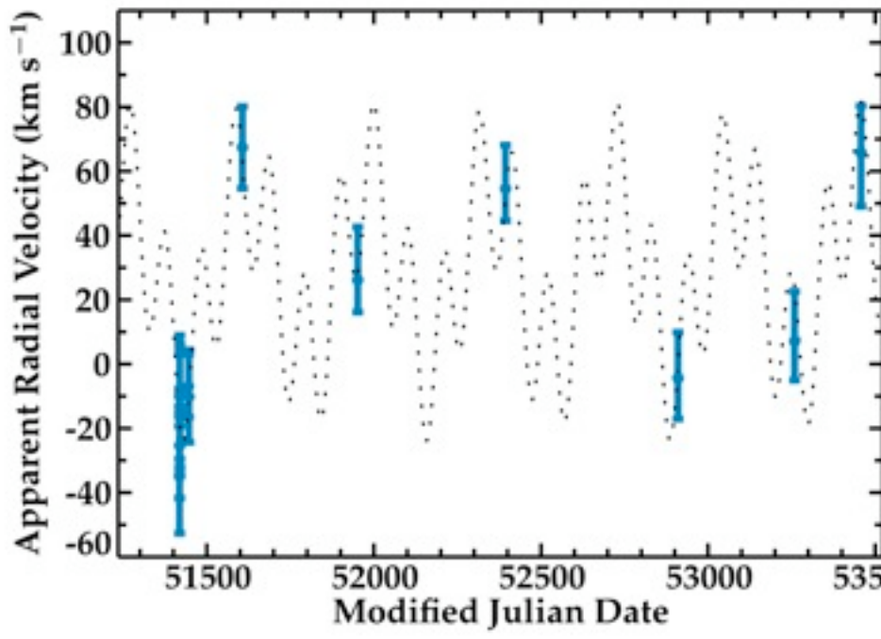

FIG. 1.—Apparent radial velocities of Capella measured with the *Cha* HETGS. The dotted line shows the calculated apparent radial motion of Ca Aa viewed from Earth (including the barycentric, orbital, and systemic m of Capella Aa); 3 σ error bars are shown in the plot.

Wood & Ayres 1995
Young et al., 2001
Ishibashi et al., 2006

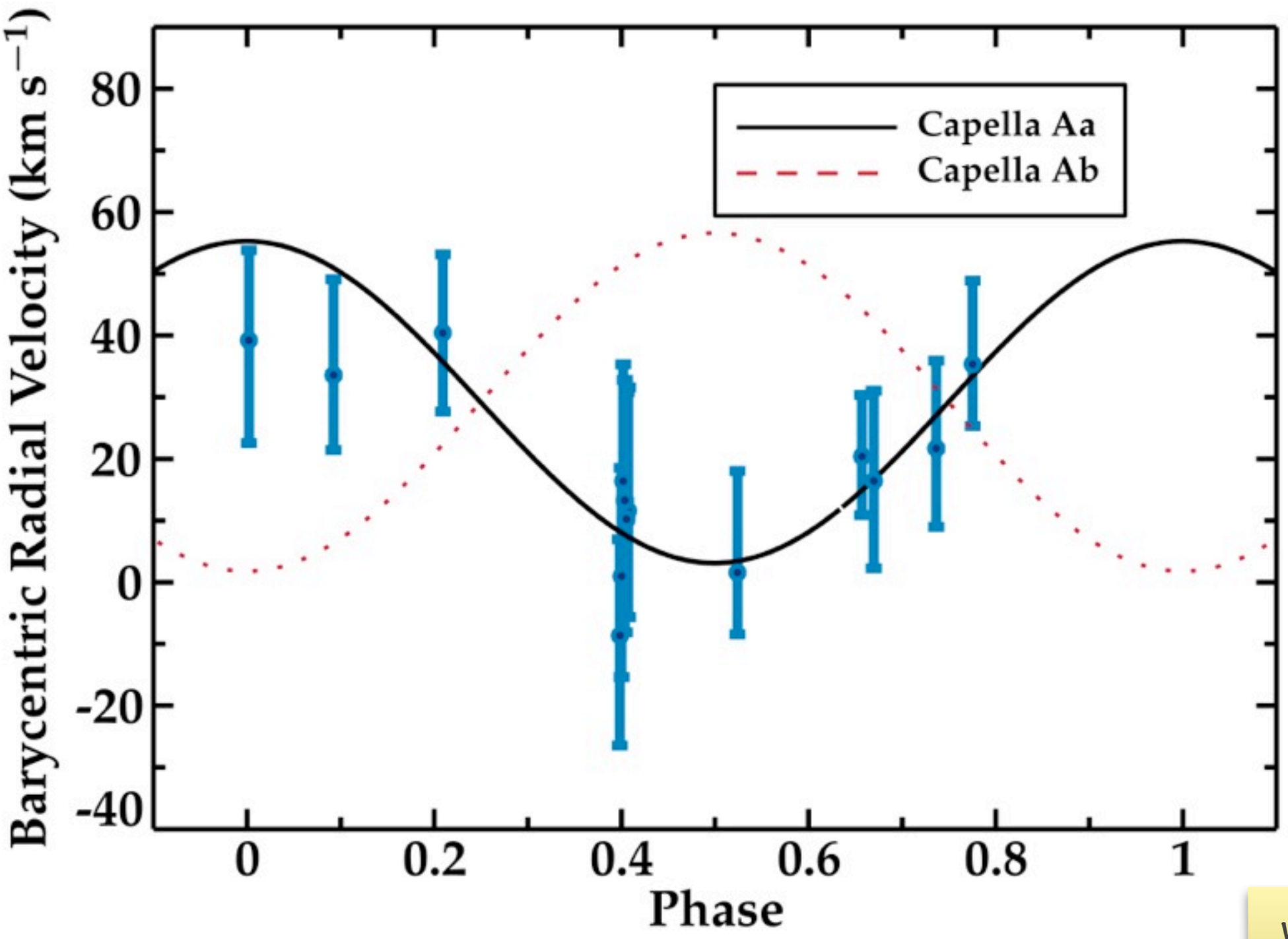

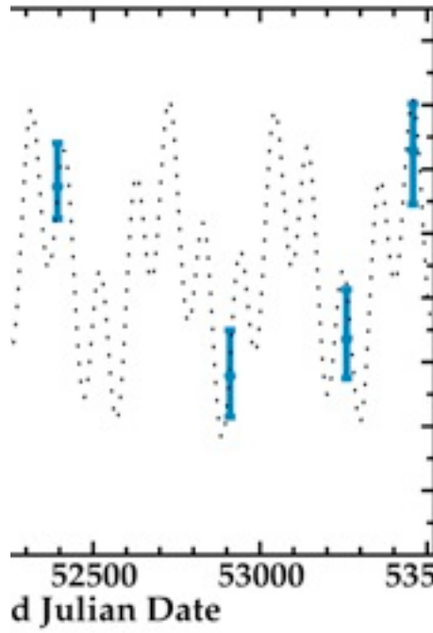

of Capella measured with the *Cha*
ulated apparent radial motion of Ca
arycentric, orbital, and systemic m
own in the plot.

Wood & Ayres 1995
Young et al., 2001
Ishibashi et al., 2006

FIG. 2.—Observed radial motion of Capella vs. orbital phase after b
centric correction (see the seventh column in Table 1). The measured radial velocity clearly follows the trend of Capella Aa (primary); 3 σ error bars are shown in the plot.

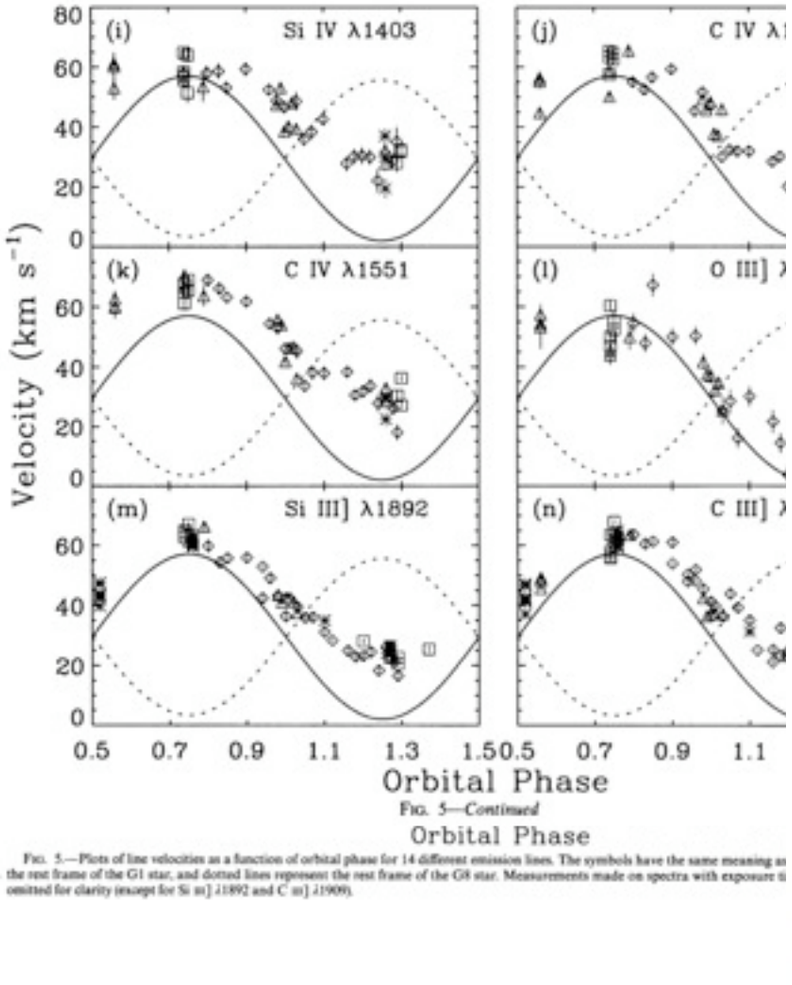

FIG. 5.—*Continued*

FIG. 5.—Plots of line velocities as a function of orbital phase for 14 different emission lines. The symbols have the same meaning as the rest frame of the G1 star, and dotted lines represent the rest frame of the G8 star. Measurements made on spectra with exposure ti omitted for clarity (except for Si III] λ1892 and C III] λ1909).

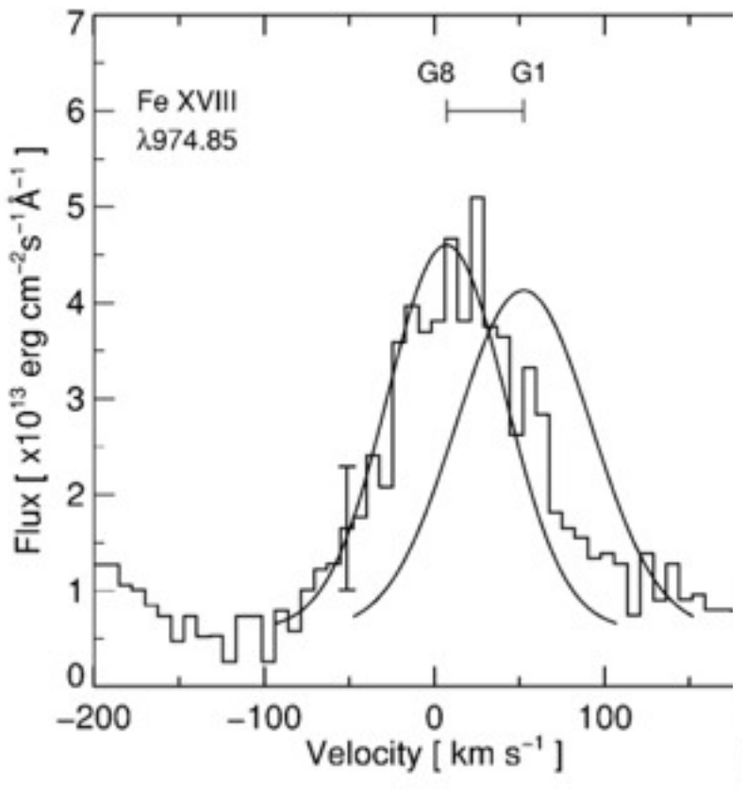

FIG. 3.—Fe XVIII λ974 profile from the SiC2A spectrum of the 20 vember 5 observation. The zero point of the velocity scale corresponds t rest wavelength of the line, determined from interstellar C III absorption at 977 Å. The expected velocities of the Capella giants are shown, together with two model profiles centered at the two stars' velocities. These model profiles show the appearance of the Fe XVIII line if it originated solely in one of the two stars, and thus they demonstrate the dominant contribution from the G8 giant. The model profiles are broadened with the thermal width of line λ974 (79 km s^{-1}), the *FUSE* instrumental broadening (20 km s^{-1}), and the rotational broadenings of each star (3 km s^{-1} for the G8 giant and 36 km s^{-1} for the G1 giant). A 1 σ error bar is also shown.

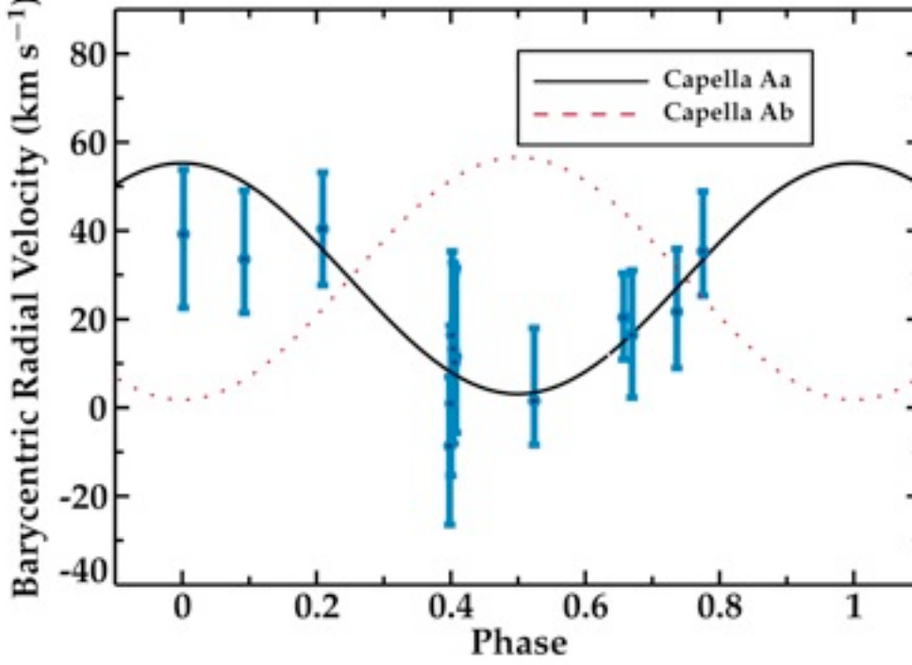

FIG. 2.—Observed radial motion of Capella vs. orbital phase after ba centric correction (see the seventh column in Table 1). The measured rad velocity clearly follows the trend of Capella Aa (primary); 3 σ error bars shown in the plot.

Wood & Ayres 1995
Young et al., 2001
Ishibashi et al., 2006

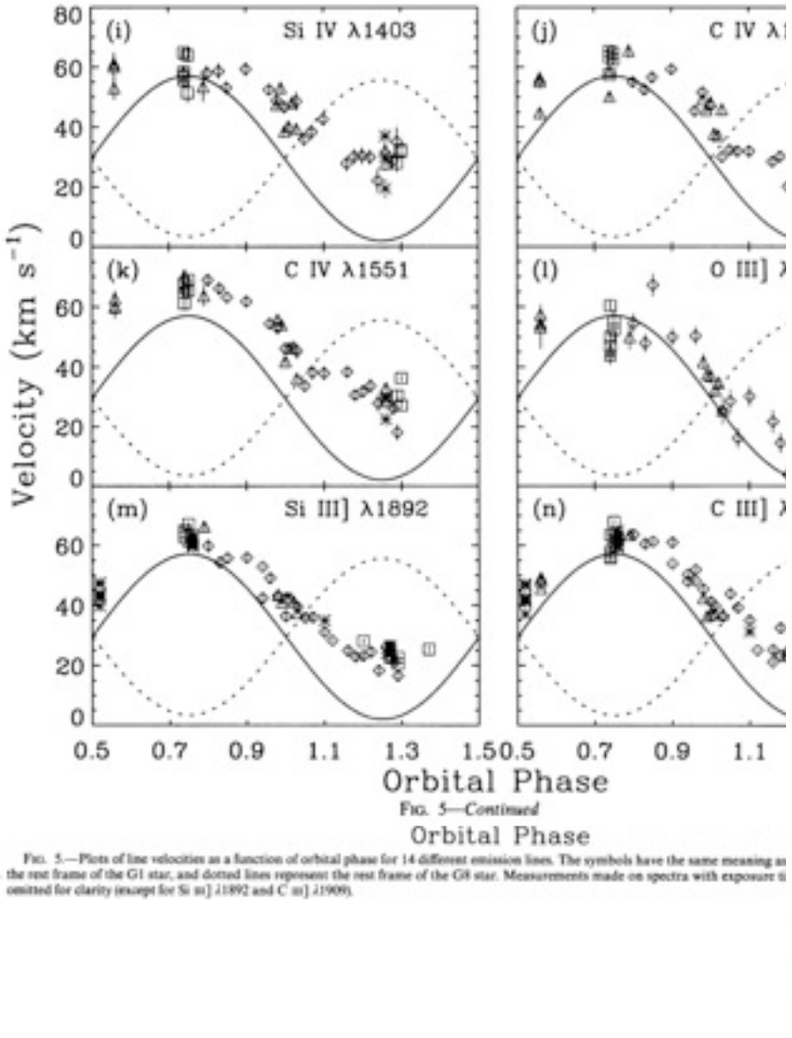

FIG. 5.—*Continued*

FIG. 5.—Plots of line velocities as a function of orbital phase for 14 different emission lines. The symbols have the same meaning as the rest frame of the G1 star, and dotted lines represent the rest frame of the G8 star. Measurements made on spectra with exposure ti omitted for clarity (except for Si III] λ1892 and C III] λ1909).

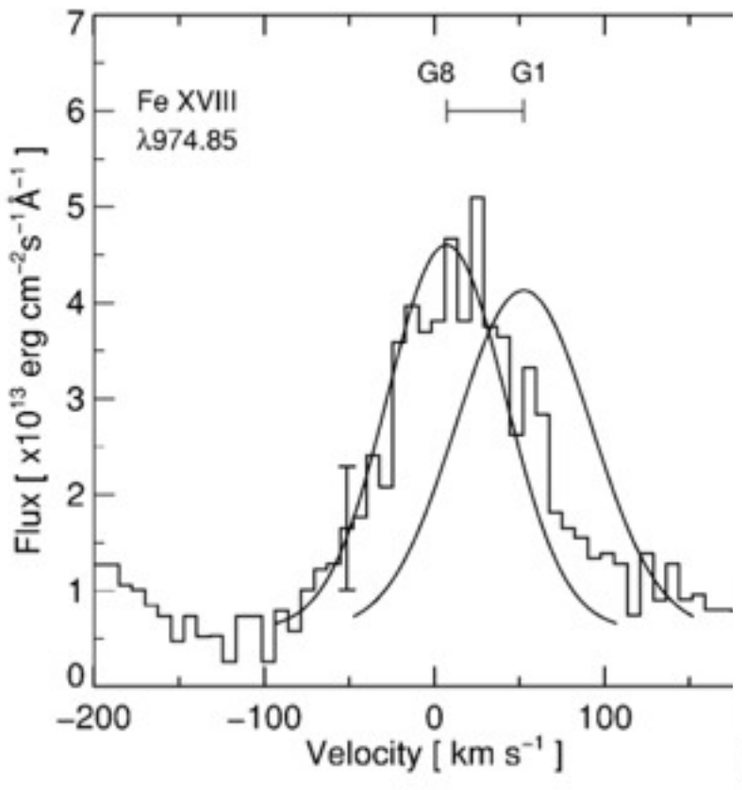

FIG. 3.—Fe XVIII λ974 profile from the SiC2A spectrum of the 20 vember 5 observation. The zero point of the velocity scale corresponds t rest wavelength of the line, determined from interstellar C III absorption at 977 Å. The expected velocities of the Capella giants are shown, together with two model profiles centered at the two stars' velocities. These model profiles show the appearance of the Fe XVIII line if it originated solely in one of the two stars, and thus they demonstrate the dominant contribution from the G8 giant. The model profiles are broadened with the thermal width of line λ974 (79 km s^{-1}), the *FUSE* instrumental broadening (20 km s^{-1}), and the rotational broadenings of each star (3 km s^{-1} for the G8 giant and 36 km s^{-1} for the G1 giant). A 1 σ error bar is also shown.

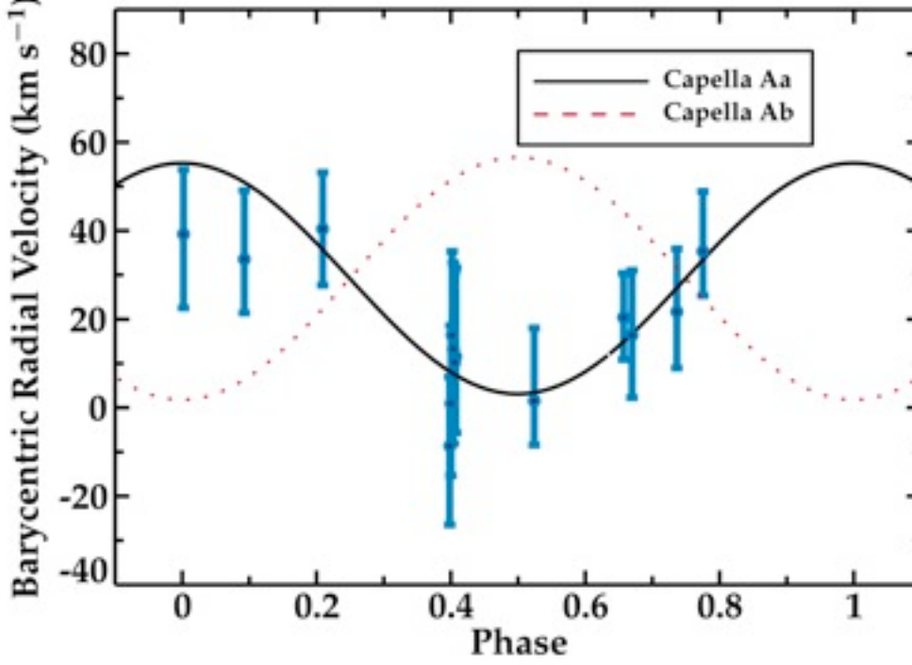

FIG. 2.—Observed radial motion of Capella vs. orbital phase after ba centric correction (see the seventh column in Table 1). The measured rad velocity clearly follows the trend of Capella Aa (primary); 3 σ error bars shown in the plot.

So: G1 dominates in UV, G8 in X-ra

Wood & Ayres 1995
Young et al., 2001
Ishibashi et al., 2006

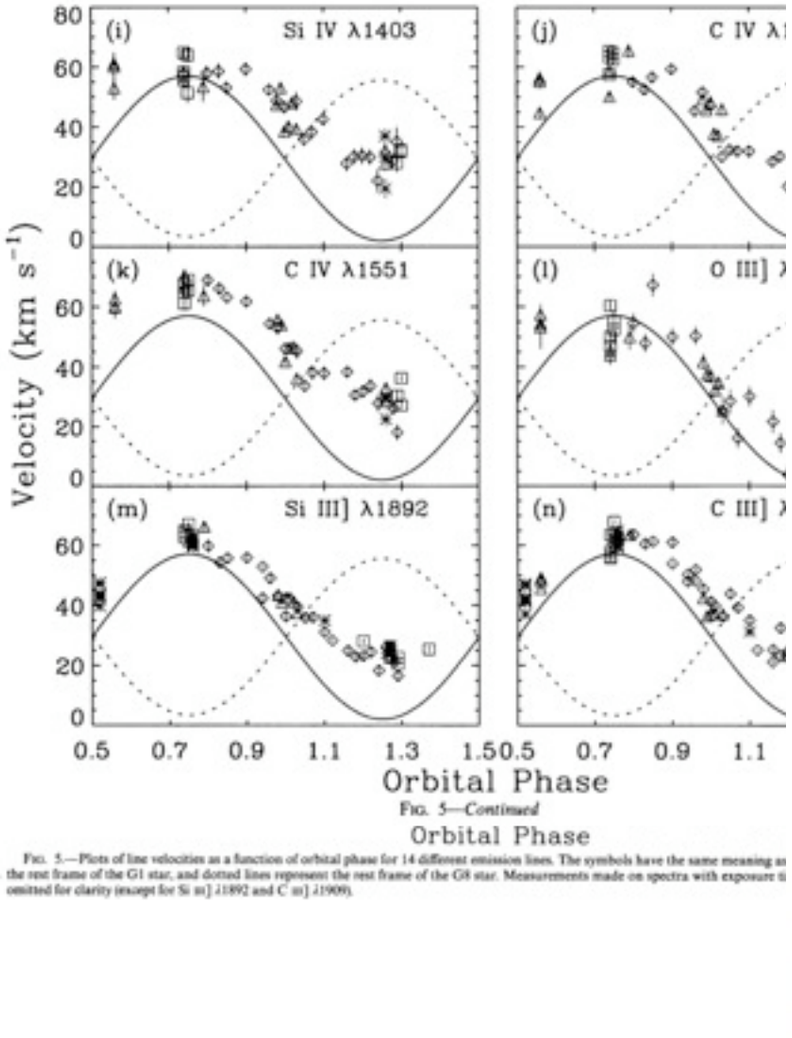

FIG. 5.—*Continued*

FIG. 5.—Plots of line velocities as a function of orbital phase for 14 different emission lines. The symbols have the same meaning as the rest frame of the G1 star, and dotted lines represent the rest frame of the G8 star. Measurements made on spectra with exposure ti omitted for clarity (except for Si III] λ1892 and C III] λ1909).

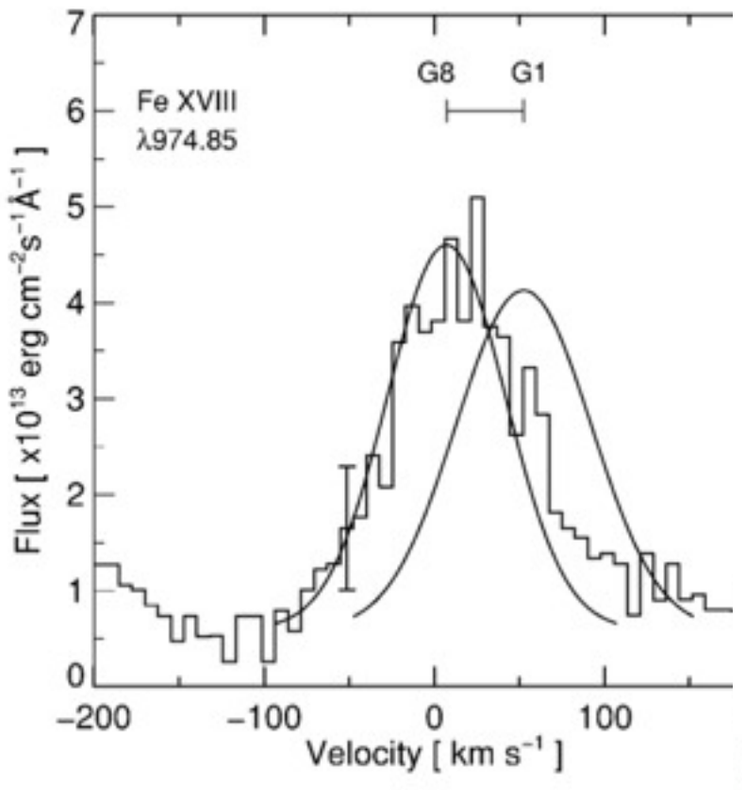

FIG. 3.—Fe XVIII λ974 profile from the SiC2A spectrum of the 20 vember 5 observation. The zero point of the velocity scale corresponds t rest wavelength of the line, determined from interstellar C III absorption at 977 Å. The expected velocities of the Capella giants are shown, together with two model profiles centered at the two stars' velocities. These model profiles show the appearance of the Fe XVIII line if it originated solely in one of the two stars, and thus they demonstrate the dominant contribution from the G8 giant. The model profiles are broadened with the thermal width of line λ974 (79 km s^{-1}), the *FUSE* instrumental broadening (20 km s^{-1}), and the rotational broadenings of each star (3 km s^{-1} for the G8 giant and 36 km s^{-1} for the G1 giant). A 1 σ error bar is also shown.

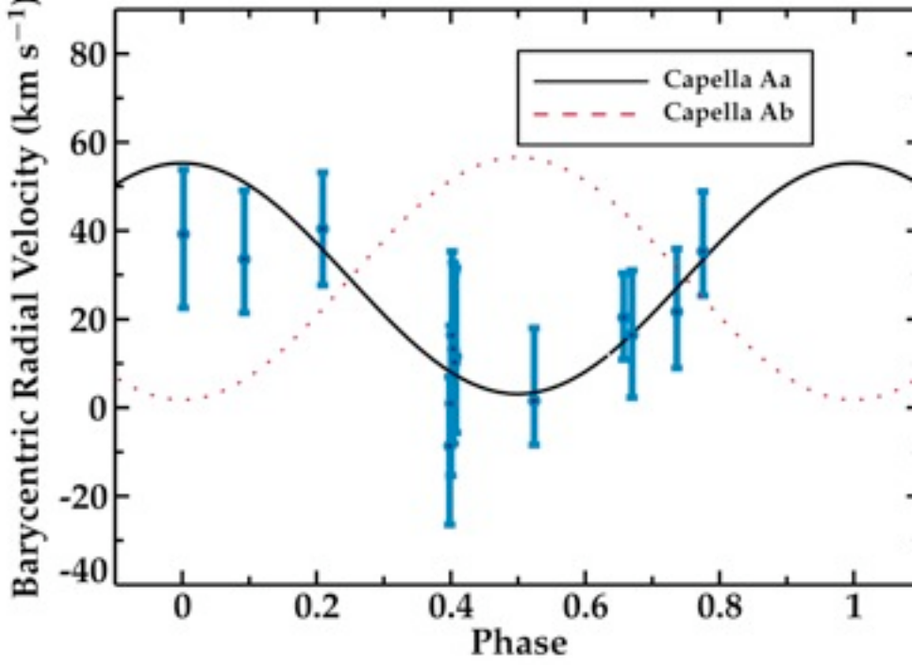

FIG. 2.—Observed radial motion of Capella vs. orbital phase after ba centric correction (see the seventh column in Table 1). The measured rad velocity clearly follows the trend of Capella Aa (primary); 3 σ error bars shown in the plot.

So: G1 dominates in UV, G8 in X-ra

not so fast..

Wood & Ayres 1995
Young et al., 2001
Ishibashi et al., 2006

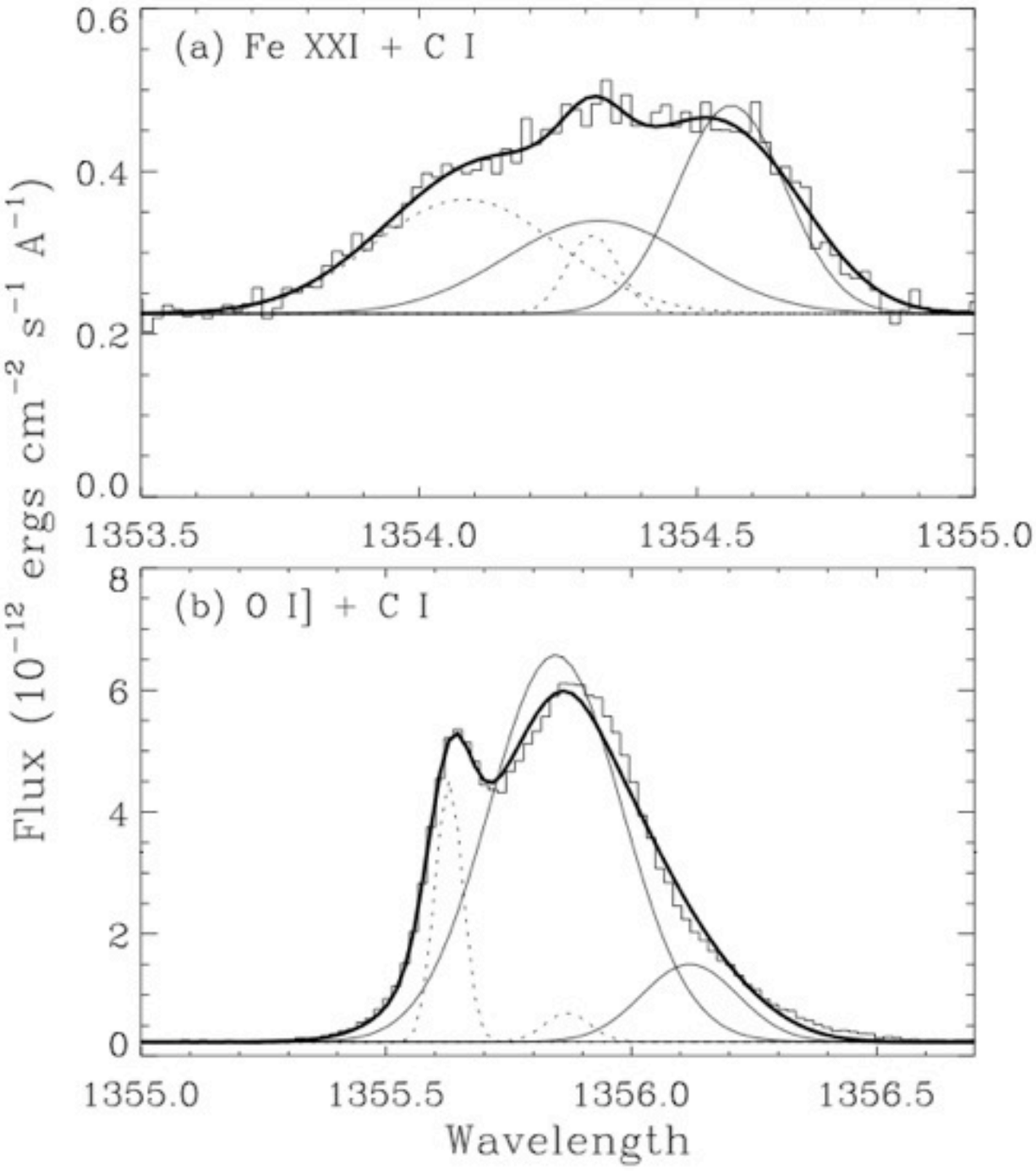

Linsky et al., 1998
Johnson et al., 2002

FIG. 3.—(*a*) Four-Gaussian fit to the Fe XXI + C I blend. C I emission from the G8 and G1 stars. The solid (dotted) lines are the G1 (G8) star's Fe XXI and C I lines, where the Fe XXI emission is to the left. The thick solid line is the sum of the four Gaussians convolved with the instrumental and rotational broadening profiles. (*b*) Four-Gaussian fit to the O I] + C I blend. Analogous to (*a*), the solid (dotted) lines are the G1 (G8) star's O I] and C I lines, with the O I] line to the left.

Linsky et al., 1998
Johnson et al., 2002

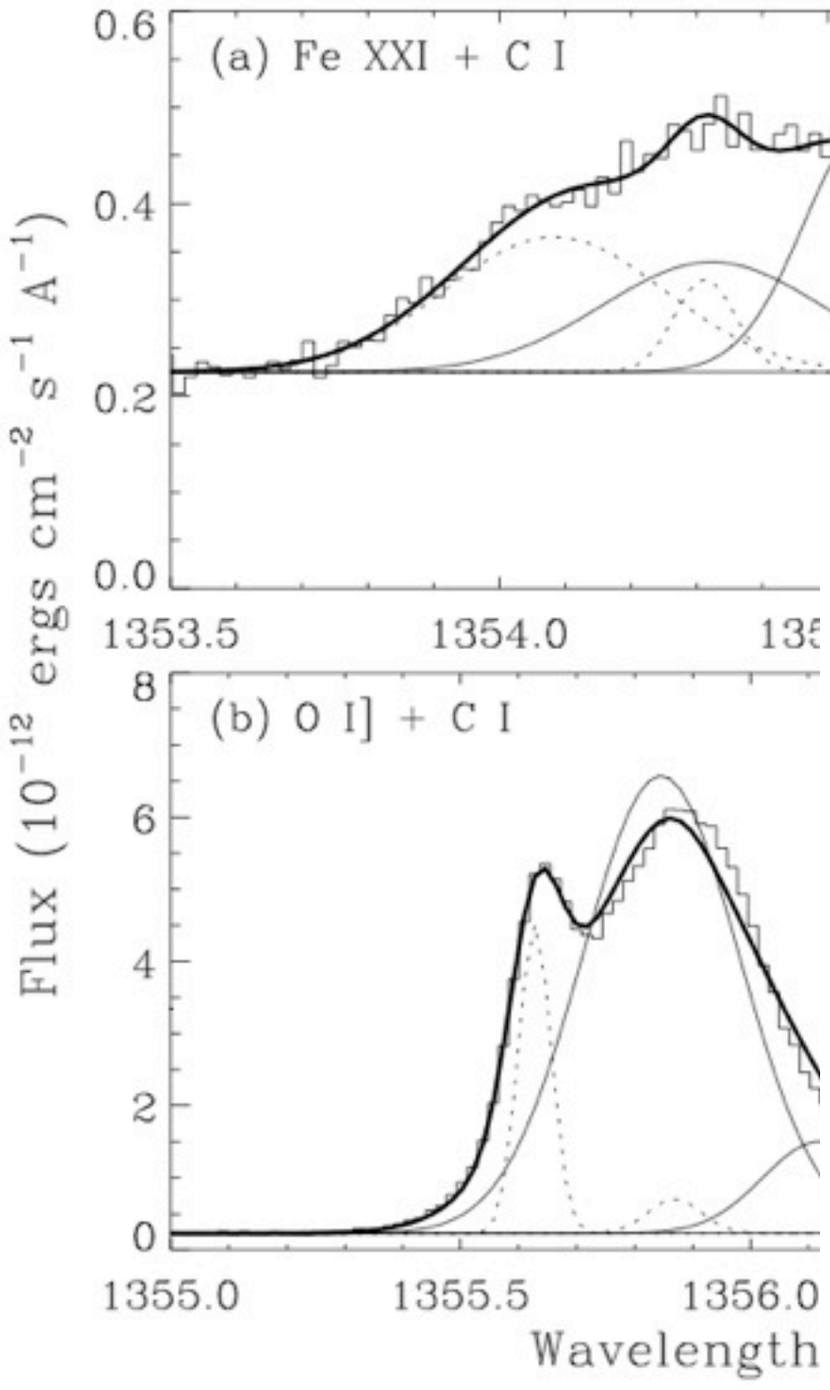

FIG. 3.—(*a*) Four-Gaussian fit to the Fe XXI · from the G8 and G1 stars. The solid (dotted) lines XXI and C I lines, where the Fe XXI emission is t line is the sum of the four Gaussians convolved v rotational broadening profiles. (*b*) Four-Gaussi blend. Analogous to (*a*), the solid (dotted) lines a and C I lines, with the O I] line to the left.

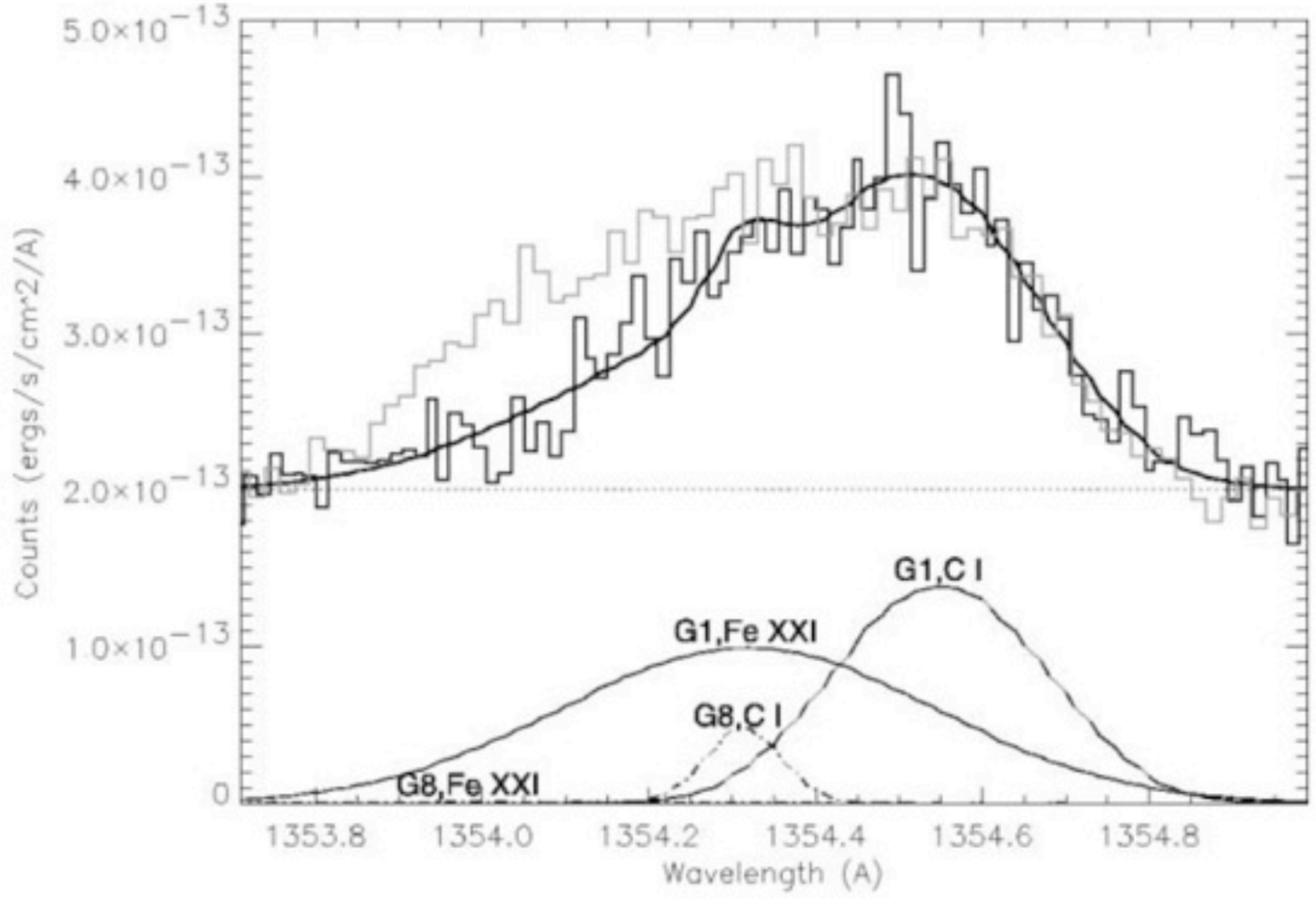

FIG. 2.—Fit to the C I/Fe XXI blend at 1354 Å. Our *HST* STIS data are represented by the thick histogram, the composite fits by the thick curve, the G1 components by the thin curve, and the G8 components by the dotted curve. Overplotted by the gray histogram are the 1995 September 9 *HST* GHRS data presented by Linsky et al. (1998), with the fluxes decreased by a factor of 1.225 to account for the presumed lowered efficiency of our observations.

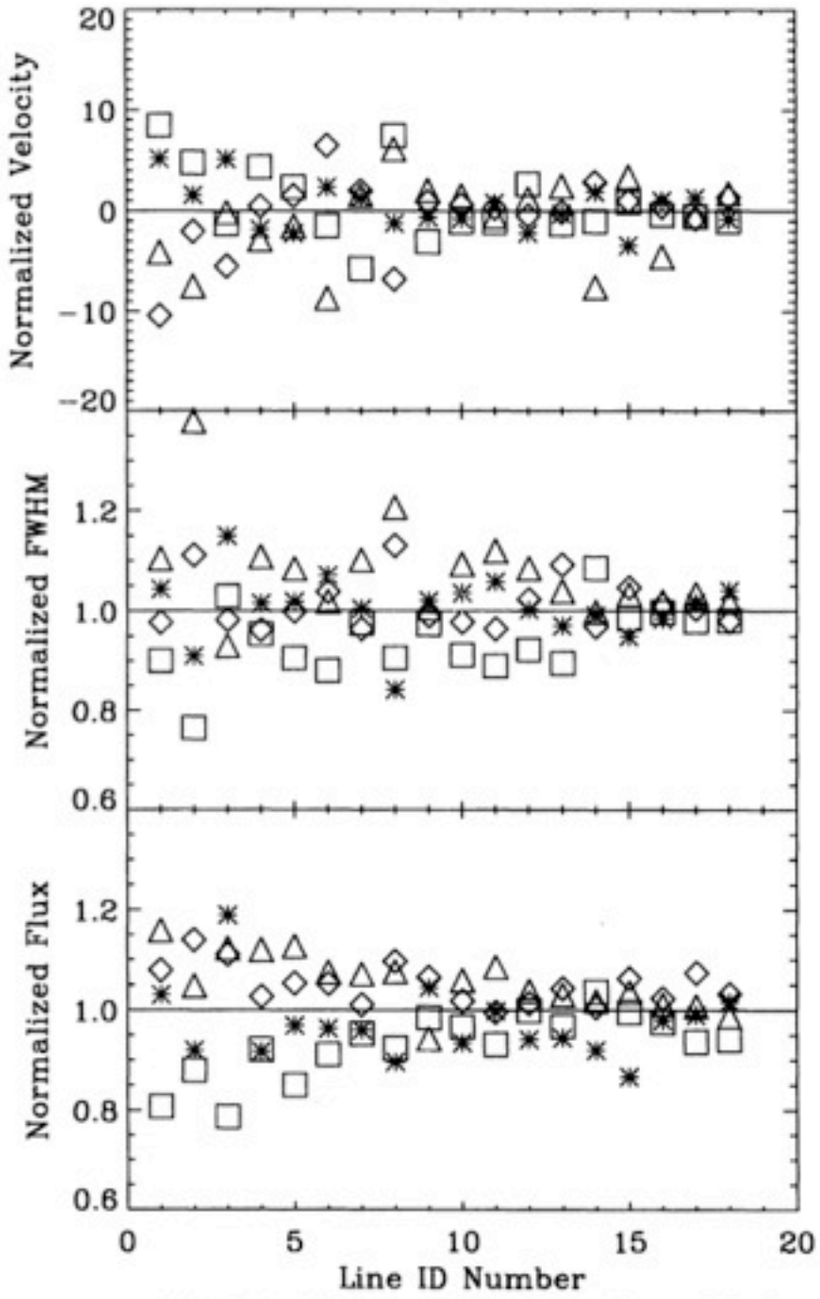

FIG. 4.—We divided the 106 *IUE* spectra into four time periods: images 1–23 (*asterisks*), 24–65 (*diamonds*), 66–88 (*triangles*), and 89–106 (*squares*). For each group we have computed average line profile parameters for the 18 lines listed in Table 2 and normalized them to the values in Table 2.

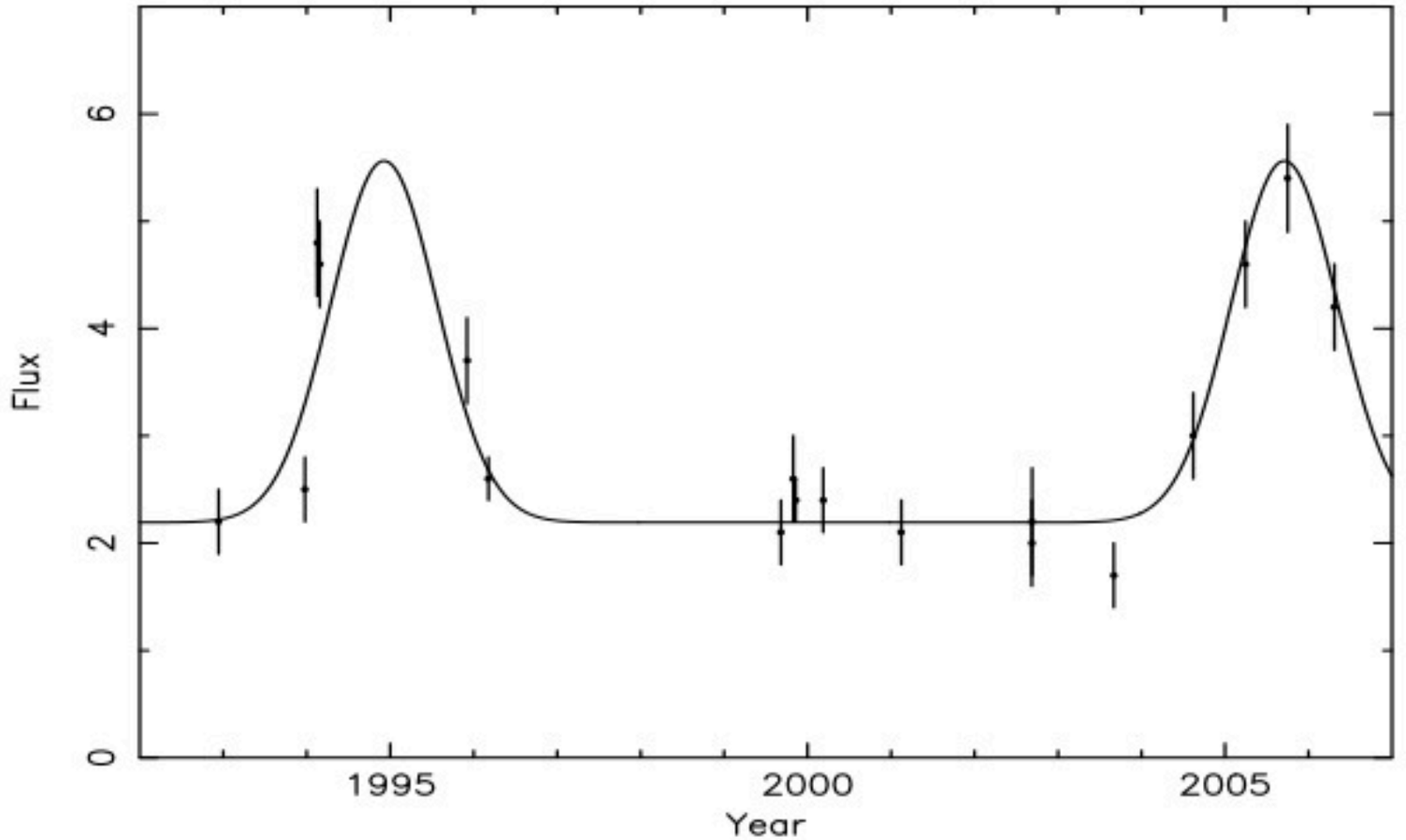

g. 5. The line flux of Fe XXI line $\lambda = 128.73$ versus time. Over
urs 1992 to 1995 we use the data from *EUVE* (Linsky et al. 1998),
e data point in 1996 from *EUVE* (Brickhouse et al. 2000) and o
years 1999 to 2005 we use the data from *LETGS* aboard *CHAND*
is work). The fluxes are in units of 10^{-13} erg cm^{-2} s^{-1}.

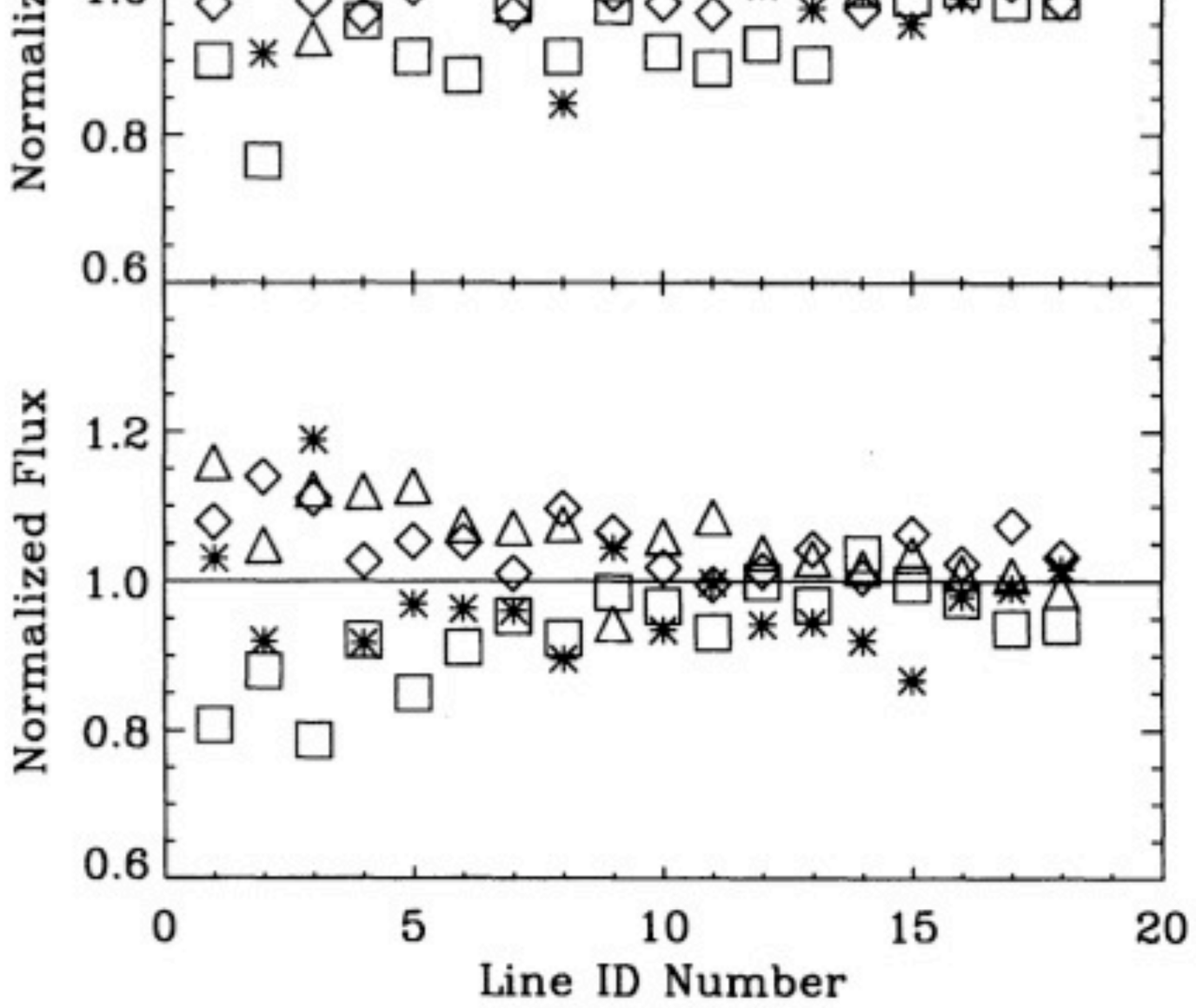

FIG. 4.—We divided the 106 *IUE* spectra into four time periods: images 1–23 (*asterisks*), 24–65 (*diamonds*), 66–88 (*triangles*), and 89–106 (*squares*). For each group we have computed average line profile parameters for the 18 lines listed in Table 2 and normalized them to the values in Table 2.

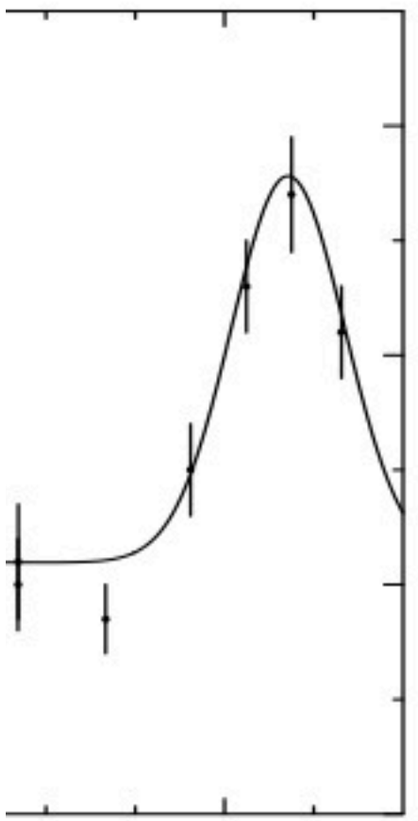

versus time. Over
insky et al. 1998),
et al. 2000) and c
S aboard *CHAND*
n^{-2} s^{-1}.

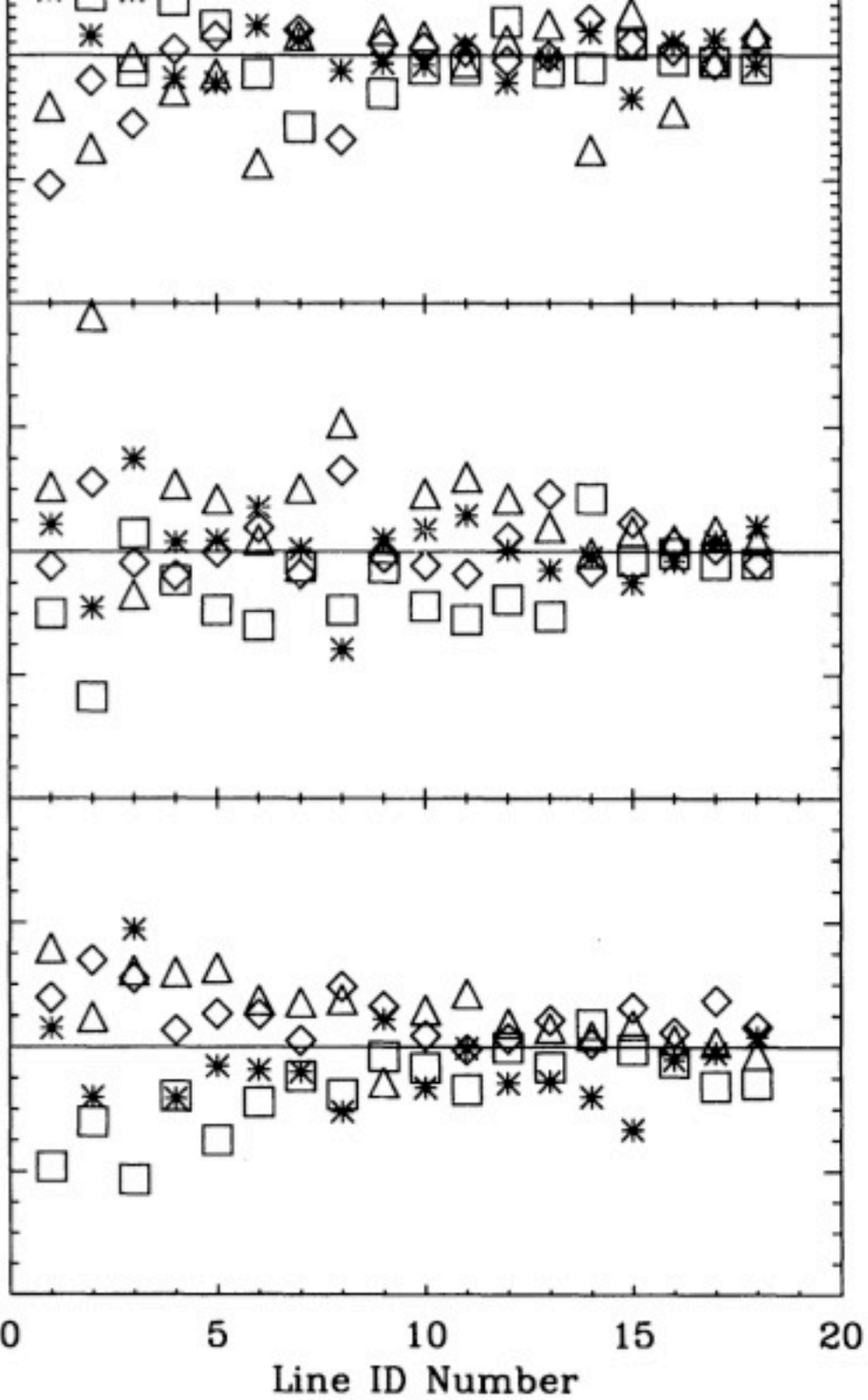

Ve divided the 106 *IUE* spectra into four time periods: images
s), 24–65 (*diamonds*), 66–88 (*triangles*), and 89–106 (*squares*). For
e have computed average line profile parameters for the 18 lines
e 2 and normalized them to the values in Table 2.

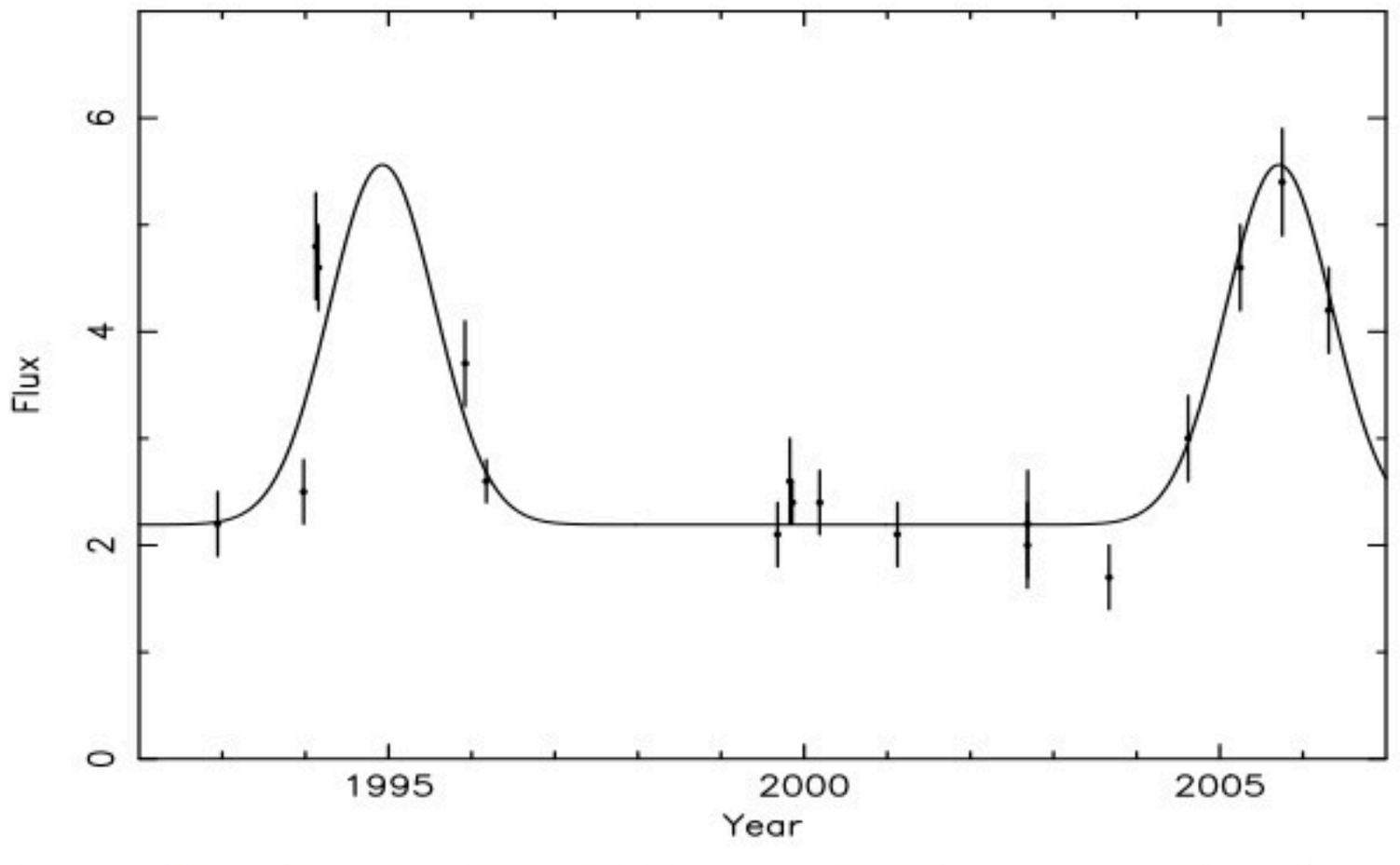

5. The line flux of Fe XXI line $\lambda = 128.73$ versus time. Over
s 1992 to 1995 we use the data from *EUVE* (Linsky et al. 1998),
data point in 1996 from *EUVE* (Brickhouse et al. 2000) and c
ears 1999 to 2005 we use the data from *LETGS* aboard *CHAND*
work). The fluxes are in units of 10^{-13} erg cm^{-2} s^{-1}.

Capella HRC−S/LETG Zeroeth Order

Flux [photons/s/cm^2]

0.10
0.09
0.08
0.07
0.06
0.05

20
40
60
80
100
120
140

Time [Months Since Jan 1999]


06540 (+5 d)
06543 (+5 d)
06544 (+5 d)
06541 (+6 d)
06542 (+6 d)
06545 (+18 d)
06546 (+18 d)
06553 (+18 d)
06547 (+21 d)
06548 (+21 d)
06554 (+21 d)
−3 mm
−12 mm
−15 mm
−6 mm
−9 mm
−18 mm
−21 mm
21 mm
3 mm
6 mm
45 mm
06554 (+21 d)
06549 (+23 d)
06550 (+23 d)
06551 (+23 d)
06552 (+23 d)
06555 (+39 d)
06556 (+39 d)
06557 (+40 d)
06558 (+40 d)
06559 (+40 d)
45 mm
9 mm
12 mm
15 mm
18 mm
48 mm
51 mm
54 mm
57 mm
08341 (+409 d)
08342 (+409 d)
08343 (+409 d)
08344 (+409 d)
08345 (+411 d)
08346 (+411 d)
08347 (+411 d)
08348 (+412 d)
08349 (+412 d)
08350 (+412 d)
−57 mm
−54 mm
−51 mm
−48 mm
−45 mm
−42 mm
−39 mm
−36 mm
−33 mm
−30 mm
08350 (+412 d)
08351 (+412 d)
08352 (+412 d)
08353 (+412 d)
08354 (+412 d)
08355 (+412 d)
08356 (+415 d)
08357 (+415 d)
08358 (+415 d)
08359 (+416 d)
08360 (+416 d)
−30 mm
−27 mm
−24 mm
24 mm
27 mm
30 mm
33 mm
36 mm
39 mm
42 mm
0 mm
Cumulative exposure [ks]

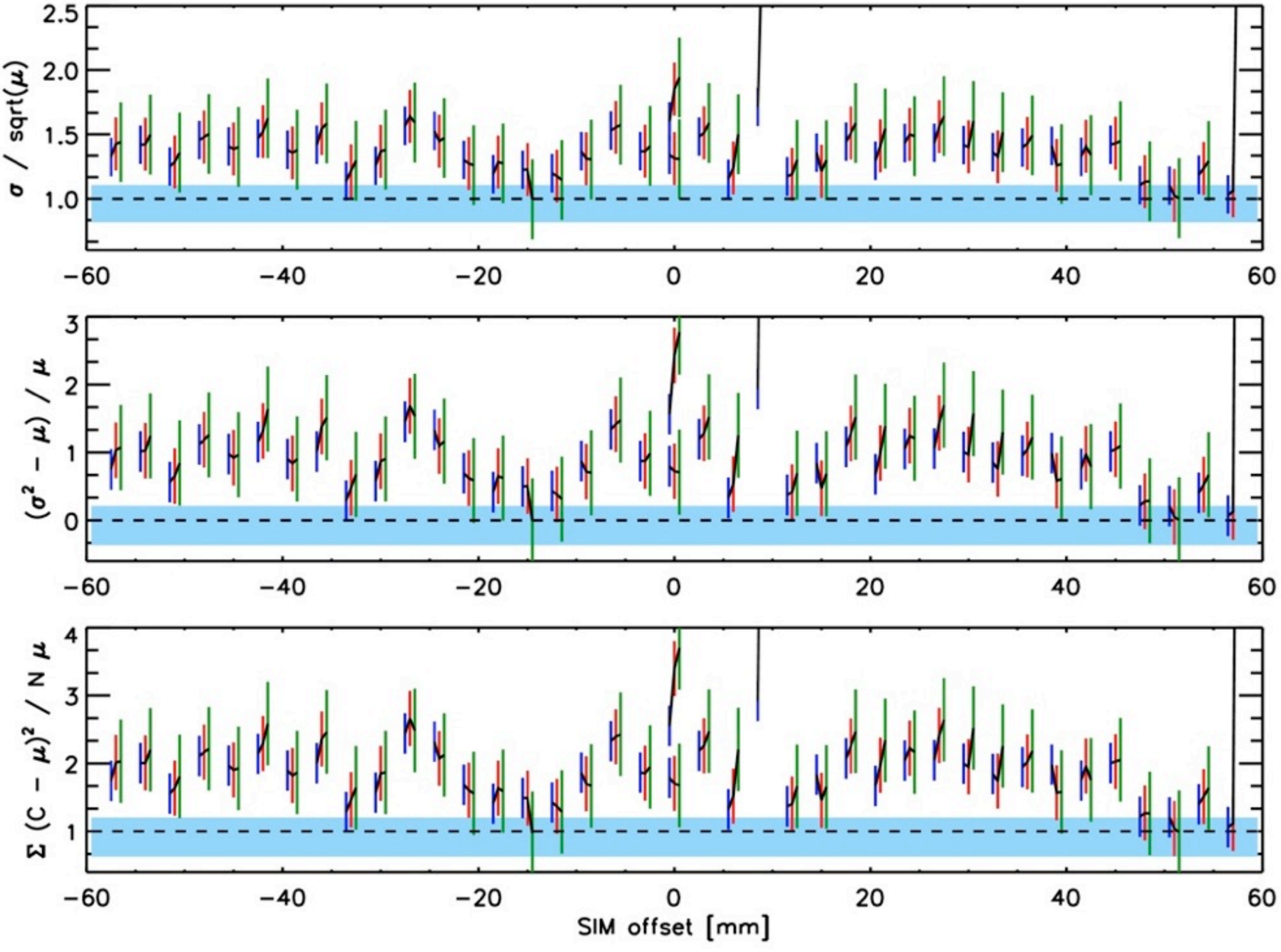
σ / sqrt(μ)
2.5
2.0
1.5
1.0
−60
−40
−20
0
20
40
60
(σ² − μ) / μ
3
2
1
0
Σ (C − μ)² / N μ
4
3
2
1
SIM offset [mm]

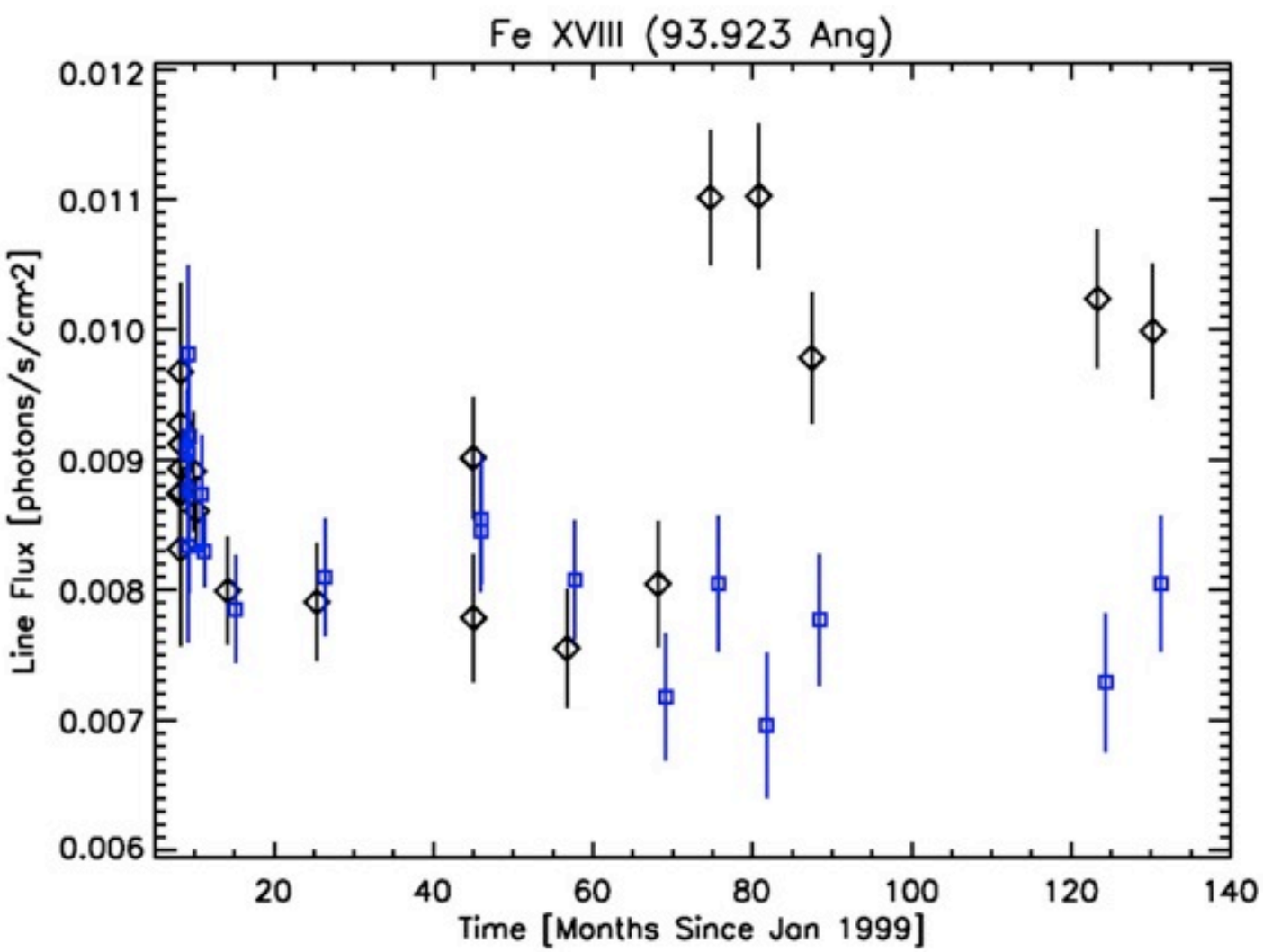
Fe XVIII (93.923 Ang)
Line Flux [photons/s/cm^2]
0.012
0.011
0.010
0.009
0.008
0.007
0.006
20
40
60
80
100
120
140
Time [Months Since Jan 1999]

Fe XVIII (93.923 Ang)

Fe XVII (17.051 Ang)

Line Flux [photons/s/cm^2]

Time [Months Since Jan 1999]

Fe XVIII (93.923 Ang)

Line Flux [photons/s/cm^2]

0.012
0.011
0.010
0.009
0.008
0.007

Fe XVII (17.051 Ang)

Line Flux [photons/s/cm^2]

0.016
0.014
0.012
0.010
0.008

20 40 60 80 100

Time [Months Since Jan 1999]

Ne IX (13.500 Ang)

Line Flux [photons/s/cm^2]

0.0045
0.0040
0.0035
0.0030
0.0025

20 40 60 80 100 120 140

Time [Months Since Jan 1999]

Fe XVIII (93.923 Ang)

Line Flux [photons/s/cm^2]

0.012
0.011
0.010
0.009
0.008
0.007

Fe XXII (117.170 Ang)

Line Flux [photons/s/cm^2]

0.004
0.003
0.002
0.001

Fe XVII (17.051 Ang)

Line Flux [photons/s/cm^2]

0.016
0.014
0.012
0.010
0.008

20 40 60 80 100

Time [Months Since Jan 1999]

Ne IX (13.500 Ang)

Line Flux [photons/s/cm^2]

0.0045
0.0040
0.0035
0.0030
0.0025

20 40 60 80 100 120 140

Time [Months Since Jan 1999]

O VII (22.101 Ang)

Line Flux [photons/s/cm^2]

0.0016
0.0014
0.0012
0.0010
0.0008
0.0006

20 40 60 80 100 120 140

Time [Months Since Jan 1999]

Fe XXII (117.170 Ang)

Ne IX (13.500 Ang)

Line Flux [photons/s/cm^2]

0.014
0.012
0.010
0.008

20 40 60 80 100

Time [Months Since Jan 1999]

Line Flux [photons/s/cm^2]

0.0040
0.0035
0.0030
0.0025

20 40 60 80 100 120 140

Time [Months Since Jan 1999]

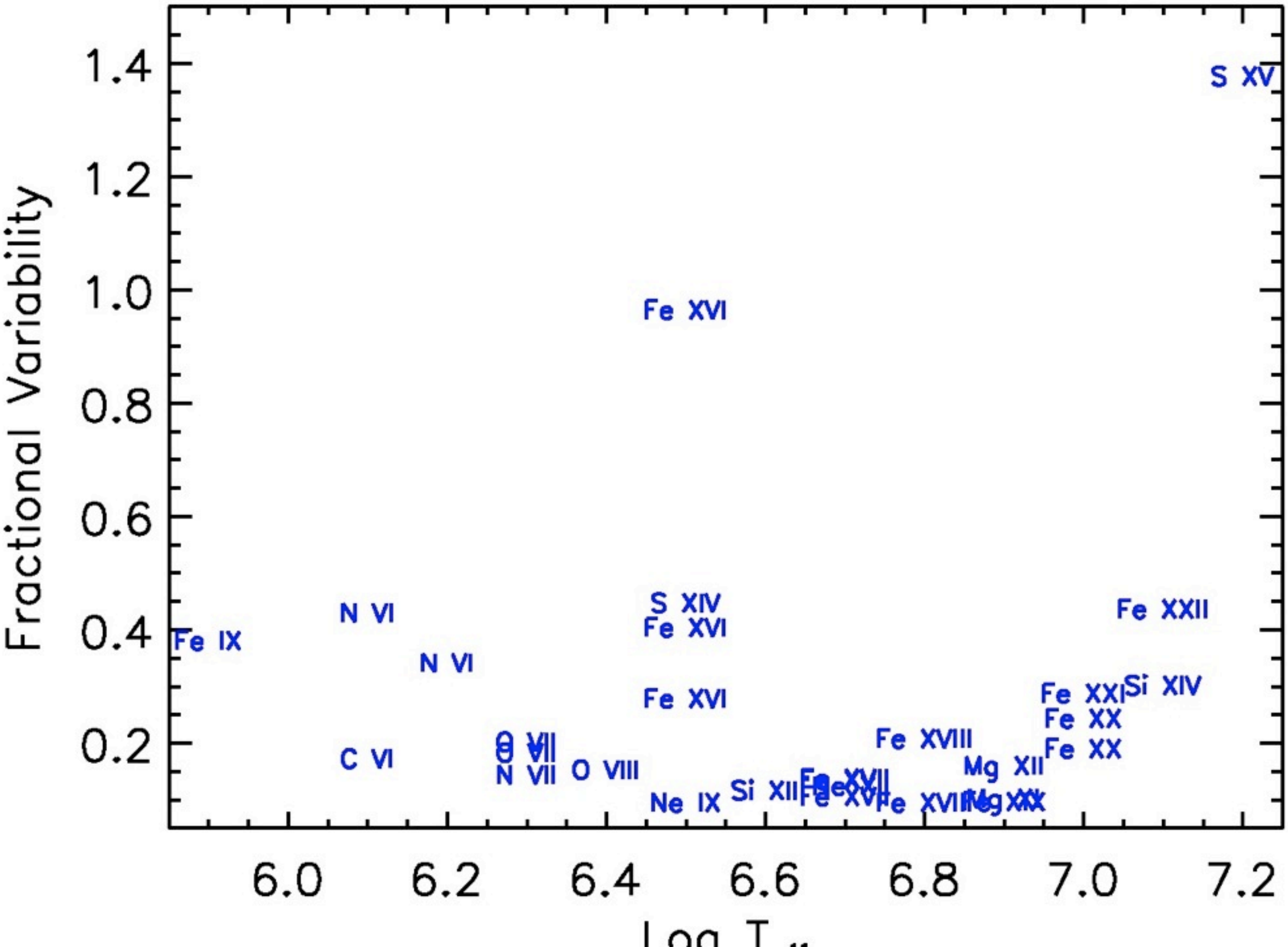
Fractional Variability
1.4
1.2
1.0
0.8
0.6
0.4
0.2
6.0
6.2
6.4
6.6
6.8
7.0
7.2
Log T
S XV
Fe XVI
Fe IX
N VI
N VI
S XIV
Fe XVI
Fe XVI
C VI
O VII
O VII
N VII
O VIII
Ne IX
Si XII
Fe XVII
Fe XVIII
Fe XVII
Mg XII
Fe XXII
Si XIV
Fe XXI
Fe XX
Fe XX

Reduced Chi−Square

10

1

O VIII
Fe XVII
Fe XVII
Fe XVII
Fe XVI
Fe XVI
Fe XVIII
O VII
O VII
Ne X
Fe XXII
Fe XVIII
Fe XXI
Fe IX
C VI
Fe XVI
Ne IX
Si XII
Fe XIX
N VII
Mg XII
Si XIV
N VI
S XIV
Fe XX
N VI
S XV

6.0 6.2 6.4 6.6 6.8 7.0 7.2

Log T_e

Summary

Summary

- Capella is a simple, bright, line dominated source that makes a great calibration target

Summary

- Capella is a simple, bright, line dominated source that makes a great calibration target
- But

Summary

- Capella is a simple, bright, line dominated source that makes a great calibration target
- But
  - difficult to separate out contributions due to components

Summary

- Capella is a simple, bright, line dominated source that makes a great calibration target
- But
  - difficult to separate out contributions due to components
  - line shifts due to Doppler velocity shifts

Summary

- Capella is a simple, bright, line dominated source that makes a great calibration target
- But
  - difficult to separate out contributions due to components
  - line shifts due to Doppler velocity shifts
  - luminosity variations at short (~5 ks) and long (~year) timescales

Summary

- Capella is a simple, bright, line dominated source that makes a great calibration target
- But
  - difficult to separate out contributions due to components
  - line shifts due to Doppler velocity shifts
  - luminosity variations at short (~5 ks) and long (~year) timescales
  - complex temperature variations with fulcrum at 6 MK

Summary

- Capella is a simple, bright, line dominated source that makes a great calibration target
- But
  - difficult to separate out contributions due to components
  - line shifts due to Doppler velocity shifts
  - luminosity variations at short (~5 ks) and long (~year) timescales
  - complex temperature variations with fulcrum at 6 MK
- We don't know why the coronae of Capella are the way they are

Summary

- Capella is a simple, bright, line dominated source that makes a great calibration target
- But
  - difficult to separate out contributions due to components
  - line shifts due to Doppler velocity shifts
  - luminosity variations at short (~5 ks) and long (~year) timescales
  - complex temperature variations with fulcrum at 6 MK
- We don't know why the coronae of Capella are the way they are
  - why no flares?

Summary

- Capella is a simple, bright, line dominated source that makes a great calibration target
- But
  - difficult to separate out contributions due to components
  - line shifts due to Doppler velocity shifts
  - luminosity variations at short (~5 ks) and long (~year) timescales
  - complex temperature variations with fulcrum at 6 MK
- We don't know why the coronae of Capella are the way they are
  - why no flares?
  - what is special about 6 MK?

Summary

- Capella is a simple, bright, line dominated source that makes a great calibration target
- But
  - difficult to separate out contributions due to components
  - line shifts due to Doppler velocity shifts
  - luminosity variations at short (~5 ks) and long (~year) timescales
  - complex temperature variations with fulcrum at 6 MK
- We don't know why the coronae of Capella are the way they are
  - why no flares?
  - what is special about 6 MK?
  - could it be continuous microflaring?

Summary

- Capella is a simple, bright, line dominated source that makes a great calibration target
- But
  - difficult to separate out contributions due to components
  - line shifts due to Doppler velocity shifts
  - luminosity variations at short (~5 ks) and long (~year) timescales
  - complex temperature variations with fulcrum at 6 MK
- We don't know why the coronae of Capella are the way they are
  - why no flares?
  - what is special about 6 MK?
  - could it be continuous microflaring?
- The work of the hi-res WG will help to calibrate the star

Capella (α Aur) - HP 24608

Magnitude: **0.05** B-V: 0.79
Absolute Magnitude: -0.51
RA/DE J2000 : 5h16m41.4s/+45° 59'51.9"
RA/DE of date : 5h17m27s/+46° 0'30"
Hour angle/DE: 23h30m6s/+46° 0'30"
Az/Alt: +53° 2'54"/+83°30'33"
Spectral Type: M1:_comp
Distance: 42.20 Light Years
Parallax: 0.07729"

+285° +60° +270° +255° +240° +225° +210° +195° +60° +50°

Taurus

Orion

Perseus

+315°

Cassiopeia

Auriga

+330°

Camelopardalis

Gemini

+345° +40°

+15° +30° +45° +60° +75° +90°